Identifying a superimposed porphyry-epithermal system based on alteration-mineralization mapping: example from the Cretaceous Dongnan Cu deposit, Zijinshan ore district (SE China)

Gan Duan
School of Earth, Atmosphere and Environment, Monash University, Australia

Huayong Chen
Key Laboratory of Mineralogy and Metallogeny, Guangzhou Institute of Geochemistry, Chinese Academy of Sciences, PRChina

Abstract. The temporal evolution of alteration in porphyry-epithermal systems has been well established based on a porphyry-centered system, with high-sulfidation (HS) epithermal deposits overlapping the porphyry system (telescoping), or adjacent to a deeper porphyry deposit. There is still conjecture on the origin of hydrothermal fluids responsible for telescoped deposits, especially where multiple hydrothermal events occur. The Dongnan Cu (-Mo) deposit with both HS and porphyry alteration, located around 1 km to the southeast of Zijinshan HS epithermal deposit and around 1.5 km to the southwest of Luoboling porphyry deposit within the Zijinshan ore district (ZOD), offers a window to investigate the origins of hydrothermal fluids responsible for these mineralization-alteration events in such porphyry-epithermal mineral systems. Detailed field and drill logging and alteration mineral mapping by shortwave infrared spectroscopy analysis (SWIR) show that HS-type alteration decreases from west to east in the ZOD, whilst the east part of ZOD is dominated by porphyry-type alteration. The distribution of alteration minerals indicates that the hydrothermal fluids for the porphyry-type and HS-type alteration at Dongnan deposit come separately from east and west, suggesting that multiple magmatic centers exist in the ZOD, which contributes to the understanding of ore genesis of this superimposed porphyry-epithermal system and supports further mineral exploration in the Zijinshan Ore district.

1 Introduction

The large-size Zijinshan porphyry-epithermal Cu-Au-Mo-Ag ore district is located in the southwestern Fujian Province of Southeast China (Fig. 1; So et al. 1998) and in the Circum-Pacific porphyry metallogenic domain (Gao et al. 2018). By the end of 2014, the proven reserves in the Zijinshan ore district comprise 400 t Au, 4.14 Mt Cu, 6339 t Ag and 0.11 Mt Mo (Zhang 2013). The Zijinshan Cu-Au mineralization, as the first recognized Cretaceous HS epithermal deposit in mainland China, hosts a reserve of 3 Mt Cu (0.36%) and 300 t Au (0.2g/t ~ 0.5g/t) (Zhang 2013). The Luoboling deposit is currently the largest porphyry deposit in the ZOD, with proven reserves of 1.4 Mt Cu (0.39%) and 0.11 Mt Mo (0.036%; Zhang, 2013). The newly discovered and currently explored Dongnan Cu (-Mo) deposit is located between the Zijinshan deposit and the Luoboling deposit (Duan et al. 2017), showing both HS epithermal deposit and porphyry deposit characteristics, with a current estimated reserve of about 0.1 Mt contained Cu metal at 0.4% and 3,000 t Mo at 0.012% (Zijin Mining Group Co. 2014).

Previous research has been mainly dedicated to the famous Zijinshan and Luoboling deposits (Huang et al., 2018; Zhong et al. 2018), which generated a great wealth of data on fluid inclusions, stable isotope geochemistry, geochronology and structural geology (So et al. 1998; Jiang et al. 2013; Piquer et al. 2017;). It is now widely accepted that the Zijinshan deposit is a HS epithermal Cu-Au deposit, whilst the Luoboling deposit is a porphyry Cu-Mo deposit (Zhong et al. 2014; Zhong et al. 2018). However, a key question for the ZOD is whether the porphyry and HS mineralization processes are associated with a single fluid subjected to changing physical conditions, or by a series of superimposed events that involved multiple fluid sources from different magmatic centers (Blundy et al. 2015; Weis et al. 2012; Wilkinson 2013).

In this study, we used detailed drill hole logging data and alteration mineral SWIR mapping to refine the understanding of hydrothermal fluids responsible for both epithermal and porphyry characteristic minerals from Dongnan deposit. We consider that multiple magmatic fluids came separately from Zijinshan deposit and Luoboling deposit and resulted in telescoping of multiple alteration events at Dongnan deposit. It provides important clues not only to the relationships between porphyry and HS deposits, but also serves as an example where porphyry and epithermal deposits are spatially connected, yet they may ultimately originate from different magmatic-hydrothermal sources.

2 Regional geology

The ZOD is located in the Cathaysia Fold Belt, southeast China (Fig. 1a). Many different deposit types have been identified so far, such as the Zijinshan HS epithermal Cu-Au deposit (So et al. 1998; Zhang et al. 2003), the Luoboling porphyry Cu-Mo deposit (Zhong et al. 2011),

the Yueyang low-sulfidation (LS) epithermal Ag-Au-Cu deposit (Zhong et al. 2018), the Wuziqilong Cu deposit (Chen et al. 2011), the Ermiaogou Cu-Au deposit (Lin et al. 2012), and the Longjiangting Cu deposit (Fig. 1b ; Chen et al. 2015).

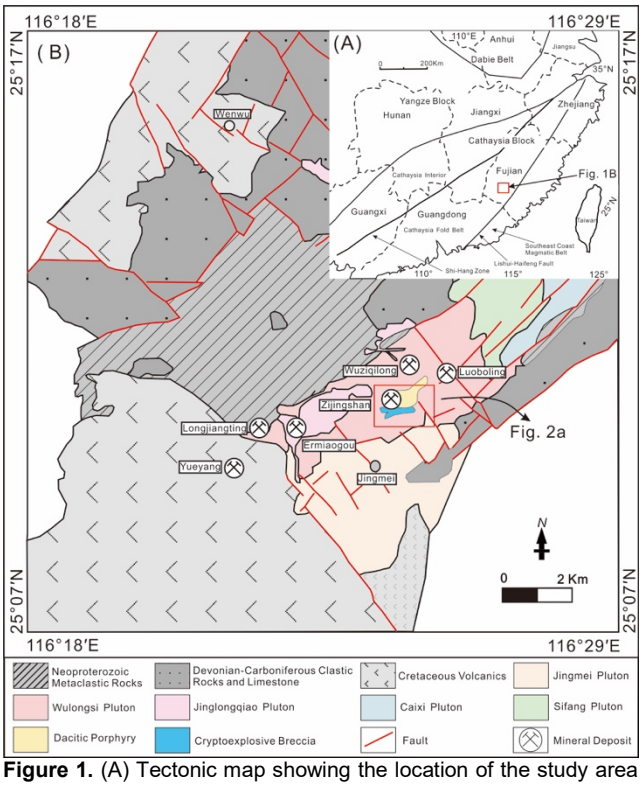

Figure 1. (A) Tectonic map showing the location of the study area (modified after Mao et al. 2013). (B) Regional tectonic framework of the ZOD (modified after Jiang et al. 2013).

The exposed strata in the ZOD consist of Neoproterozoic phyllite and fine-grained meta-sandstone unconformably overlain by Devonian-Carboniferous clastic rocks and limestone (Fig. 1b). Early Cretaceous volcanic rocks crop out in the northwestern part of the ore district and in the Shanghang Volcanic Basin (Zhang et al. 2001). Middle to Late Jurassic and Early Cretaceous magmatic rocks dominate the ore district (Zhang et al. 2001; Jiang et al. 2013). The Middle Jurassic Zijinshan granite complex in the southeastern part of the ore district, which hosts the Zijinshan HS epithermal deposit, comprises the multiphase Jingmei, Wulongsi, and Jinglongqiao granitic plutons (Zhang et al. 2001). Late Jurassic Caixi monzogranite (Yu et al. 2013) in the northeastern part of the ore district intruded the Wulongsi pluton (Mao et al. 2004). The Early Cretaceous NNE-trending Sifang granodiorite (Jiang et al. 2013) exposed in the northeastern ZOD was emplaced into the Wulongsi and Caixi plutons (Zhang et al. 2001). The Cretaceous Luoboling granodiorite porphyry in the northeastern Zijinshan ore district intruded the Sifang granodiorite (Fig. 1c; Zhang et al. 2001).

3 Geology of the Dongnan deposit

The Dongnan deposit is located between the Zijinshan and Luoboling deposits (Fig. 1b), and NW- and NNE-trending faults are very common in the study area (Figs. 1b and 2a).

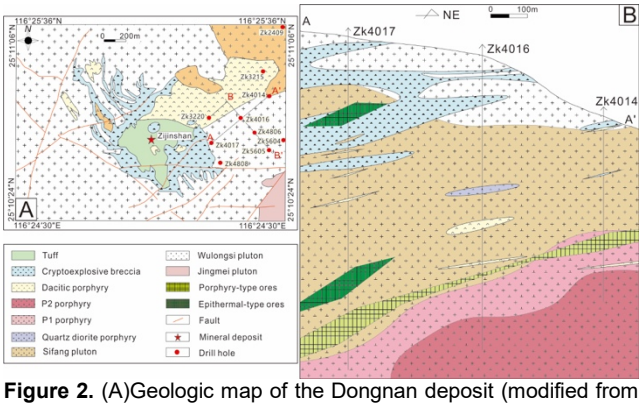

Figure 2. (A)Geologic map of the Dongnan deposit (modified from the Zijin Mining Group, 2014). (B) The NE-trending sketch profile of the Dongnan deposit.

Two major magmatic episodes have been identified at Dongnan, including a Middle to Late Jurassic (ca. 165 – 150 Ma) and a Cretaceous one which can be further divided into late Early Cretaceous (ca. 110 – 105 Ma) and early Late Cretaceous (ca. 100 – 95 Ma). The Middle to Late Jurassic rocks include the Caixi monzogranite and Wulongsi granite. The late Early Cretaceous rocks include the Sifang granodiorite, Luoboling granodiorite porphyry, quartz diorite porphyry and dacite porphyry, whilst the early Late Cretaceous rocks include rhyodacite and rhyolite. These igneous rocks show clear temporal and spatial relationships in the Dongnan deposit area (Fig. 2). The plutons exposed are mainly the Wulongsi granite and its intruding Sifang granodiorite (Figs. 2a and 2b), with the latter being intruded by the Luoboling pluton at depth (Fig. 2b). Stocks of quartz diorite porphyry and dacite porphyry are also present, with the former intruding the Sifang granodiorite and the latter intruding all the Sifang granodiorite, the Wulongsi pluton and Luoboling granodiorite porphyry (Fig. 2b; Duan et al. 2017). It is noticeable that Wulongsi granite has been severely brecciated at west Dongnan deposit due to intense hydrothermal fluid events.

In order to outline mineralization and alteration distribution of Dongnan deposit, a total of ten drill holes (around 6.8 km length in total) were chosen for detailed mineralization and alteration logging. These drill holes are distributed almost evenly in Dongnan deposit (Fig. 2a), thus can outline main mineralization and alteration zonation within Dongnan deposit. Two alteration and mineralization types (porphyry and HS epithermal) were recognized from these drill holes in field, of which the porphyry-type occurs in the Luoboling granodiorite porphyry and Sifang granodiorite stocks, and the HS epithermal-type occurs in the Sifang granodiorite and the hydrothermal breccia at shallow level (Fig. 2b). Both porphyry-type and epithermal-type ores occur as lenses, in which the former is ca. 600 m long and 30 to 50 m wide, and the latter is ca. 200 m long and 50 m wide (Fig. 2b). Porphyry-type mineralization mainly occurs as disseminated ore and quartz-sulfide veins (quartz +

chalcopyrite + pyrite + molybdenite + muscovite ± anhydrite ± K-feldspar). HS epithermal-type mineralization mainly occurs as disseminated ore (covellite + digenite + pyrite ± dickite ± alunite ± pyrophyllite).

4 Distribution of alteration minerals based on SWIR analysis

Since hydrothermal alteration at the Dongnan deposit significantly overlaps with each other, it is hard to strictly separate different alteration minerals merely by field observation. In order to solve this problem, SWIR analysis was carried out to help identify different hydrothermal alteration minerals. Around 160 samples (systematically spaced at 10 m to 50 m intervals) from six drill holes in cross sections A-A' and B-B' were used for TerraSpec SWIR at the Guangzhou Institute of Geochemistry, Chinese Academy of Sciences (GIG-CAS). More details about SWIR method see Herrmann et al.(2001).

The dickite and kaolinite alteration zones overlap each other in the upper parts of the cross section, particularly in the Wulongsi pluton, hydrothermal breccia, dacite porphyry and part of the Sifang granodiorite. The kaolinite zone is much wider than the dickite zone, and it is difficult to distinguish hypogene kaolinite from supergene kaolinite. The pyrophyllite zone in section A-A' lies below the dickite zone in the Sifang granodiorite, and partly overlaps the kaolinite zone. The pyrophyllite zone in section B-B' lies slightly below but mainly overlaps the dickite zone. The alunite zone in section A-A' comprises two parts: the upper part is closely associated with the hydrothermal breccia, and alunite occurring in this zone is also within the dickite zone; the lower part has close spatial relationships with pyrophyllite alteration. The alunite zone in section B-B' also comprises two parts: the upper part (in ZK3220 and ZK4016) is closely associated with the hydrothermal breccia, whereas, the lower part (in ZK4806 and ZK5605) overlaps both the dickite and pyrophyllite zones.

Muscovite is disseminated in section A-A' and section B-B'. In both sections, muscovite mainly occurs in the Wulongsi granodiorite and the Sifang granodiorite and is a minor phase in the Luoboling granodiorite, from the surface to ca. 500 m deep. The illite zone in the section A-A' is narrow, and lies below the muscovite, pyrophyllite, dickite and kaolinite zones in the upper parts of the Luoboling granodiorite, with a minor illite zone in the upper parts of the dacite porphyry and the Sifang granodiorite. The illite zone from section B-B' comprises two parts: the upper part in the Sifang granodiorite and the lower part in the Luoboling granodiorite. It is observed that in ZK5605 the pyrophyllite and alunite zones are located approximately between the two illite zones. The illite-montmorillonite zone is in the bottom of the sections in the Luoboling granodiorite porphyry and close to the illite zone of both sections. The illite-montmorillonite zone in the shallow quartz diorite porphyry is isolated and is likely unrelated to the illite-montmorillonite zone associated with deeper plutons.

5 Discussion

In Dongnan, porphyry type alteration characterized by phyllic alteration (muscovite + quartz + pyrite) is an early alteration stage. Detailed drill core logging and mapping show that the porphyry-type orebody at Dongnan stretches northeast into the Luoboling deposit and becomes part of the main orebody of the Luoboling deposit, which indicates that the deep porphyry-type orebody at Dongnan is a peripheral part of the Luoboling deposit. It is reasonable to suggest that Luoboling porphyry deposit is responsible for Dongnan porphyry-type alteration.

It is observed that high-sulfidation epithermal alteration (e.g. alunite, dickite and pyrophyllite) only occurs in the western part of the ZOD, superimposed on the original porphyry phyllic alteration and not in the eastern part. At least two HS alteration stages exist, one is responsible for dickite + alunite alteration and another is for alunite + pyrophyllite alteration, as pyrophyllite was overprinted by dickite. The hydrothermal fluid for the areas of HS epithermal alteration may come either from Zijinshan deposit or Luoboling porphyry deposit. The pyrophyllite alteration zone in Dongnan decreases sharply from southwest to northeast, directly suggesting that the related high-sulfidation fluid comes from the southwest direction of the Dongnan deposit. Even though pyrophyllite alteration is extensively superimposed by dickite alteration in the western surface of the Dongnan deposit, the telescoped extent decreased from west to east. This decreasing trend from west to east suggests that the fluid attributed to the HS stage at Dongnan was likely derived from the western Zijinshan HS epithermal deposit. In addition, the illite surrounds pyrophyllite in horizontal level in cross-section B-B', suggesting that epithermal fluid for pyrophyllite from west in a horizontal direction rather than vertical direction. We suggest that the HS epithermal fluid from the Zijinshan deposit migrated in east direction to the Dongnan deposit and Luoboling deposit. It resulted in intense telescoping of HS alteration on the original Dongnan porphyry deposit and partly superimposed on west part of Luoboling deposit.

6 Exploration implications

The results of this study show that even though HS epithermal deposits and porphyry deposits may be different expressions of the same system, we found evidence that multiple magmatic centers may exist and are separately responsible for telescoped epithermal and porphyry mineralization systems. For the Zijinshan and Dongnan deposits, there is still considerable exploration potential for porphyry-style mineralization at depth. On a global or mining district scale, it is important to investigate whether porphyry-epithermal systems have formed form a single magmatic pluton, or separately with genetically unique magmatic centers, but subsequently telescoped. It is therefore necessary to investigate and explore for magmatic centers within high-sulfidation alteration zones (lithocaps) in known districts of porphyry mineralization.

Acknowledgements

We thank the staff of the Zijin Mining Co. Ltd. for their field assistance. This research was financially supported by the China National Funds for Distinguished Young Scientists (No.41725009).

References

Blundy J, Mavrogenes J, Tattitch B, Sparks S, Gilmer A (2015) Generation of porphyry copper deposits by gas-brine reaction in volcanic arcs. Nat Geosci 8:235–240

Chen J, Chen YJ, Zhong J, Sun Y, Li J, Qi JP, Lu YH (2011) Fluid inclusion study of the Wuziqilong Cu Deposit in the Zijinshan Ore Field, Fujian Province. Acta Petrol Sin 27:1425–1438 (in Chinese with English abstract)

Chen J, Chen YJ, Zhong J, Sun Y, Li J, Qi JP (2015) Geological and ore-fluid characteristics of Longjiangting Cu deposit in Zijinshan Ore district, Fujian Province, and their genetic implications. Mineral Deposit 34:98–118 (in Chinese with English abstract)

Duan G, Chen HY, Hollings P, Qi J, Xu C, Zhang S, Xiao B, Liu GY, Liu JM (2017) The Mesozoic magmatic sources and tectonic setting of the Zijinshan ore district, South China: Constraints from geochronology and geochemistry of igneous rocks in the Southeastern Ore Segment. Ore Geol Rev 80:800–827

Gao J, Klemd R, Zhu M, Wang X, Li J, Wan B, Xiao W, Zeng Q, Shen P, Sun J, Qin K (2018) Large-scale porphyry-type mineralization in the Central Asian metallogenic domain: a review. J Asian Earth Sci 165:7–36

Herrmann W, Blake M, Doyle M, Huston D, Kamprad J, Merry N, Pontual S (2001) Short wavelength infrared (SWIR) spectral analysis of hydrothermal alteration zones associated with base metal sulfide deposits at Rosebery and Western Tharsis, Tasmania, and Highway-Reward, Queensland. Econ Geol 96:939–955

Huang W, Liang H, Wu L, Wu J, Li J, Bao Z (2018) Asynchronous formation of the adjacent epithermal Au-Cu and porphyry Cu-Mo deposits in the Zijinshan ore district, southeast China. Ore Geol Rev 102:351–367

Jiang SH, Liang QL, Bagas L, Wang SH, Nie FJ, Liu YF (2013) Geodynamic setting of the Zijinshan porphyry-epithermal Cu–Au–Mo–Ag ore system, SW Fujian Province, China: constrains from the geochronology and geochemistry of the igneous rocks. Ore Geol Rev 53:287–305

Lin SP, Liu S, Wang CL, Huang WT, Li ZJ, Wang CZ, Qi JP, Liang HY (2012) Locating the cryptoexplosion center at Ermiaogou Cu polymetallic deposit in the Zijin Ore Field and its geological implication. Geotecton et Metallog 36:450–456 (in Chinese with English abstract)

Mao JR, Xu NZ, Hu Q, Xing GF, Yang ZL (2004) The Mesozoic rock-forming and ore-forming processes and tectonic environment evolution in Shanghang-Datian region, Fujian. Acta Petrol Sin 20:285–296 (in Chinese with English abstract)

Mao JW, Cheng YB, Chen MH, Franco P (20130 Major types and time–space distribution of Mesozoic ore deposits in South China and their geodynamic settings. Mineral Deposita 48:267–294

Piquer J, Cooke DR, Chen J, Zhang L (2017) Synextensional Emplacement of Porphyry Cu-Mo and Epithermal Mineralization: The Zijinshan District, Southeastern China. Econ Geol 112:1055–1074

So CS, Zhang DQ, Yun ST, Li DX (1998) Alteration mineralization zoning and fluid inclusions of the high sulfidation epithermal Cu-Au mineralization at Zijinshan, Fujian province, China. Econ Geol 93:961–980

Weis P, Driesner T, Heinrich CA (2012) Porphyry-copper ore shells form at stable pressure-temperature fronts within dynamic fluid plumes. Science 338:1613–1616

Wilkinson JJ (2001) Fluid inclusions in hydrothermal ore deposits. Lithos 55:229–272

Yu B, Pei RF, Qiu XP, Chen JH, Li DP, Zhang WH, Liu WY (2013) The Evolution Series of Mesozoic Magmatic Rocks in the Zijinshan Ore district, Fujian Province. Acta Geol Sin 34:437–446 (in Chinese with English abstract)

Zhang JZ (2013) Geology, exploration model and practice of Zijinshan ore concentrated area. Mineral deposita 32:757–766 (in Chinese with English abstract)

Zhong J, Chen YJ, Chen J, Qi JP, Dai MC (2018) Geology and fluid inclusion geochemistry of the Zijinshan high-sulfidation epithermal Cu-Au deposit, Fujian Province, SE China: Implication for deep exploration targeting. J Geochem Explor 184:49–65

Zhong J, Chen YJ, Pirajno F, Chen J, Li J, Qi JP, Li N (2014) Geology, geochronology, fluid inclusion and H–O isotope geochemistry of the Luoboling porphyry Cu–Mo deposit, Zijinshan Ore district, Fujian Province, China. Ore Geol Rev 57:61—77

Zijin Mining Group Co (2014) Detailed investigation plan for the Southeast Ore Segment of the Zijinshan mineral deposit in 2014. Unpublished report (in Chinese).

Asynchronous formation of the adjacent epithermal Au-Cu and porphyry Cu-Mo deposits in the Zijinshan orefield, southeast China

Wenting Huang, Huaying Liang
Key Laboratory of Mineralogy and Metallogeny, Guangzhou Institute of Geochemistry, Chinese Academy of Sciences

Abstract. Adjacent high-sulfidation epithermal (HSE) and porphyry deposits often have similar Cu-Au metal association, are co-genetic and formed contemporaneously. The Zijinshan ore field (ZOF), the largest Au producer in China, contains a series of HSE Au-Cu and porphyry Cu-Mo deposits. The new age data indicate that the main HSE Au-Cu mineralizing event occurred at ca. 113 Ma. In comparison, the adjacent porphyry Cu-Mo mineralization formed at ca. 104 Ma, ca. 9 Myr after the HSE event. The volcanic rocks associated with the HSE Au-Cu mineralization yield zircon ε_{Hf} (t) values from -4.1 to 0.3, whereas the Cu-Mo mineralized porphyry has lower zircon ε_{Hf} (t) values (-4.5 to -1.2), suggesting that the magmas that formed the latter intrusion were derived from a source containing more crustal material than the magmas associated with the HSE mineralization. The differences in the timing of mineralization and the sources of the magmas indicate that the adjacent HSE and porphyry deposits in the ZOF formed from different magmatic-hydrothermal systems that controlled the different metal associations of the mineralizing systems. The results also show that not all adjacent porphyry and epithermal deposits, especially those with different metal associations, are co-genetic.

1 Introduction

Porphyry and high-sulfidation epithermal (HSE) mineralizing systems represent important sources of Cu, Mo, and Au (eg. Heinrich et al. 1999) and are commonly closely spatially associated (e.g. Arribas et al. 1995). A genetic link has been proposed for these types of mineral deposits (e.g. Hedenquist and Lowenstern 1994). Co-genetic porphyry and HSE deposits usually have similar Cu and Au metal associations (e.g. Deyell and Hedenquist 2011) because both Cu and Au can be transported as stable chloride complexes in high-temperature saline fluids (Hemley and Hunt 1992) before they coprecipitate (e.g. Heinrich et al. 2004). Such co-genetic deposits form contemporaneously, as evidenced by ages that are within uncertainty of each other (e.g. Arribas et al. 1995).

The Zijinshan orefield (ZOF) is located in Fujian Province and is the richest Au-Cu mining area in southeast China (Zhang 2013). Several epithermal and porphyry deposits have been identified within the ZOF, including the Zijinshan HSE Au-Cu deposit, which is the largest epithermal deposit in China, and the Luoboling porphyry Cu-Mo deposit, which represents the largest porphyry deposit in southeast China (Zhang 2013). These two HSE and porphyry deposits are thought to be co-genetic, forming from the same magmatic-hydrothermal system (e.g. So et al. 1998; Zhang et al. 2001; Jiang et al. 2013). However, this co-genetic model for the ZOF is unlikely to be correct for a number of reasons. Firstly, the Zijinshan HSE deposit has an Au-Cu metal association, whereas the adjacent Luoboling porphyry deposit has a Cu-Mo metal association but contains low concentrations of Au (< 0.1 ppm). This pair of HSE Au-Cu and porphyry Cu-Mo deposits is different from the majority of adjacent and co-genetic HSE and porphyry deposits that have similar Au-Cu associations (Heinrich et al. 2004). Secondly, the co-genetic model is not supported by age data, as the porphyry mineralization is thought to have formed at ca. 104 Ma (e.g. Zhong et al. 2014), whereas the timing of epithermal mineralization remains poorly constrained.

This study presents a new robust zircon U-Pb age and muscovite ^{40}Ar-^{39}Ar ages for the Zjinshan HSE deposit to investigate the relationship between the deposits. We also determined the zircon Hf isotopic composition of a series of igneous rocks in the ZOF to understand variation in the sources of magmas associated with the deposits and their contrasting metal associations.

2 Geological setting

The ZOF is located in the eastern part of the Cathaysian fold belt in southeast China. There are two stages of magmatism, including the Late Jurassic and the Early Cretaceous, in the ZOF. The deposits in the ZOF were genetic-related with the Cretaceous magmatism (e.g. So et al. 1998; Jiang et al. 2013).

The ZOF contains numerous epithermal and porphyry deposits, including the giant Zijinshan HSE Au-Cu deposit, the large Longjiangting intermediate-sulfidation epithermal Cu-Ag-Au deposit, the large Yueyang low-sulfidation Ag-Au-Cu deposit, the small Wuziqilong Cu-Ag (Au) deposit, the large Luoboling porphyry Cu-Mo deposit, the small Jinmei porphyry Cu-Mo deposit and the Ermiaogou epithermal Cu (Au) deposit. These deposits contain a total of 399 tons of Au, 6.400 thousand tons of Ag, 4.137 million tons of Cu, and 110 thousand tons of Mo (Zhang 2013).

The Zijinshan HSE Au-Cu deposit is located in the central ZOF and is related to an early episode of Shimaoshan Group volcanism (So et al. 1998). The ore-hosting volcanic rocks have undergone pervasive hydrothermal alteration. In brief, there are four zones between the shallow and central alteration zones, and the

deeper alteration zones in the deposit, namely (1) a silicic-alteration (Q) zone, (2) an alunite-alteration (Alu-Q) zone, (3) a dickite alteration (Q-Alu-Di-Phy) zone, and (4) a sericite alteration (Phy) zone (So et al. 1998).

The Luoboling porphyry Cu-Mo deposit is located in the northeastern ZOF. Detailed geo-chronological research indicates the presence of two stages of mineralization-related granodiorite porphyry magmatism that yield zircon U-Pb ages of ca. 103 Ma and ca. 97 Ma (e.g. Huang et al. 2013).

3 Muscovite Ar-Ar ages

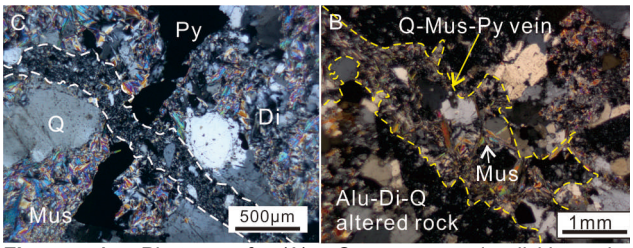

Figure 1. Photos of (A) Quartz-muscovite-dickite-pyrite assemblage cut by a quartz-alunite altered breccia, and (B) a quartz-muscovite-pyrite vein within the alunite-dickite alteration assemblage.
Abbreviations: Alu = alunite, Di = dickite, Mus = muscovite, Py = pyrite, and Q = quartz.

Sample ZJ-27 was collected from a quartz-muscovite-dickite-pyrite veinlet that is cut by quartz-alunite altered breccia (Fig. 1A) from the Q-Alu-Di-Phy zone. It yielded a flat age spectrum after stepwise laser heating. The main plateau consists of 16 successive steps (from steps 4 to 19) that represent 95.75% of the ^{39}Ar released and yield a plateau age of 113.4 ± 1.1 Ma with a MSWD of 0.25 (Fig. 2A).

Sample LJ-04 was collected from an outcropping quartz-muscovite-pyrite veinlet that cuts an alunite-dickite altered rock (Fig. 1B). Removing the first and last few steps, data for muscovite sample LJ-04 yielded a total of 17 successive steps (4 to 20) that represent 82.74% of ^{39}Ar released from the sample. These steps define the main plateau for this sample, yielding a plateau age of 110.4 ± 1.3 Ma with a MSWD of 0.12 (Fig. 2B).

Both samples yield initial ^{40}Ar/^{39}Ar values of 291 ± 14 and 292 ± 16, respectively, which are within uncertainty of the atmospheric argon value of 295.5 (Renne et al. 2009), indicating that the muscovite did not include inherited or excess ^{40}Ar. Their plateau ages (113.4 ± 1.1 Ma and 110.4 ± 1.3 Ma) are therefore interpreted to represent the timing of crystallization of the muscovite.

4 Zircon U-Pb ages

Sample ZJ1505 is from the crypto-explosive breccia (Fig. 3) and yields zircon U-Pb ages from 108.5 to 630 Ma. Two spots with U-Pb ages of 628 and 630 Ma represent inherited zircons, and a further seven zircons yield U-Pb ages of 137 - 167 Ma that may represent fragments derived from Jurassic granites. The remaining seven zircons yield a U-Pb age for the crypto-explosive breccia

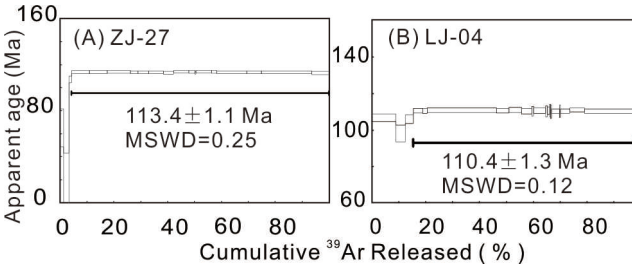

Figure 2. Apparent muscovite ^{40}Ar-^{39}Ar ages for representative samples from the Zijinshan HSE Au-Cu deposit.

of 112.9 ± 1.2 Ma with a MSWD of 0.96.

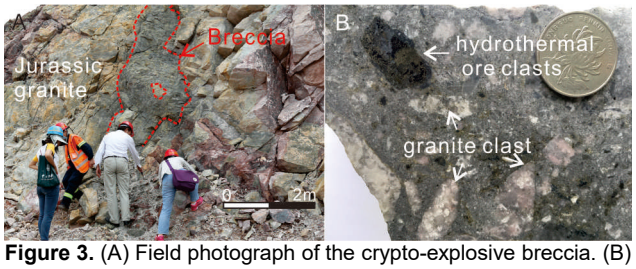

Figure 3. (A) Field photograph of the crypto-explosive breccia. (B) Representative hand sample of the crypto-explosive breccia comprising clasts of hydrothermal mineralization and Jurassic granite.

5 Zircon Hf isotopic compositions

Zircons within the crypto-explosive breccia (sample ZJ1502) yield ^{176}Hf/^{177}Hf ratios of 0.282718-0.282661 and ε_{Hf} (t) values from -1.5 to 0.5. These zircons have associated two-stage Hf model ages (T_{DM2}) of 1140 to 1268 Ma.

Zircons from the Luoboling granodiorite porphyry have ^{176}Hf/^{177}Hf ratios of 0.282583-0.282674, corresponding to ε_{Hf} (t) values from -4.5 to -1.2. Their two-stage Hf model ages range from 1214 to 1447 Ma.

6 Discussions

6.1 Asynchronous formation of porphyry and epithermal mineralization within the ZOF

Previous geochronological analysis of the Zijinshan deposit yielded four K-Ar ages on alunite from 82 to 111.7 Ma (Zhou and Chen 1996; Zhang et al. 2005), two Rb-Sr isochron ages on quartz-hosted fluid inclusions of 100 and 122 Ma (Zhou and Chen 1996), and three Rb-Sr isochron ages on whole-rock samples from 110 to 124 Ma (Chen 1996; Mao et al. 2002). The large range of these ages (from 124 to 82 Ma) suggests that both the alunite K-Ar system and the Rb-Sr system within these samples were disturbed by later hydrothermal events within the ZOF. Jiang et al. (2017) reported Re-Os model ages that range from 142 to 82 Ma for pyrite from the Zijinshan deposit (Jiang et al. 2017). This indicates that these pyrites formed over several stages of hydrothermal activity (Cardon et al. 2008).

Muscovite is a common mineral within the root zone of

porphyry Cu deposits (Seedorff et al. 2008) and in epithermal deposits. Muscovite has a radiogenic argon closure temperature of either 270°C - 325°C (Snee et al. 1988) or up to 410 °C (Hames and Bowring 1994; Kirschner et al. 1996). This means that muscovite ^{40}Ar-^{39}Ar results should more accurately record the mineralization age of an ore deposit that underwent multi-stage hydrothermal activity.

Some quartz-muscovite-pyrite veins cut the alunite-dickite alteration within the ZOF (Fig. 1B), indicating that the muscovite formed later than the alteration. This indicates that the ^{40}Ar-^{39}Ar plateau age (110.4 ± 1.3 Ma) of the muscovite represents a minimum age for the alunite-dickite alteration. This in turn indicates that the hydrothermal activity associated with the formation of the HSE Cu-Au mineralization occurred before ca. 110 Ma.

The Q-Alu-Di-Phy zone also contains disseminated muscovite and quartz-muscovite-dickite-pyrite veinlet in volcanic breccia (Fig. 1A). The planar crystal boundaries between muscovite and dickite suggest that these minerals formed contemporaneously. On a smaller scale, the quartz-muscovite-dickite-pyrite assemblage is cut by an alunite-altered breccia (Fig. 1A). These observations suggest that the epithermal mineralization-related muscovite formed contemporaneously with the dickite-alteration but earlier than the alunite-alteration. The ^{40}Ar-^{39}Ar plateau age (113.4 ± 1.1 Ma) of the muscovite therefore constrains the upper age of the alunite alteration to ca.113 Ma.

In addition, the crypto-explosive breccia, which containing clasts of hydrothermal sulfide mineralization (Fig. 3B), yields a zircon U-Pb age of 112.9 ± 1.2 Ma. It represents a minimum age for the hydrothermal sulfide ores within the deposit. The ^{40}Ar-^{39}Ar plateau age of the muscovite that is co-genetic with the dickite is within uncertainty of the zircon U-Pb age of the crypto-explosive breccia, again suggesting that the HSE Cu-Au mineralization formed at ca. 113 Ma.

Previously reported molybdenite Re-Os isochron ages of Luoboling porphyry Cu-Mo deposit is ca. 104 Ma (eg. Zhong et al. 2014). These age data indicate that the porphyry Cu-Mo mineralization formed ca. 9 Myr later than the main HSE mineralization. In other words, the adjacent HSE Au-Cu and porphyry Cu-Mo deposits within the ZOF are associated with two distinct episodes of magmatism and are not genetically linked.

6.2 Magmatic sources evolution and implications for metal associations

The various metal associations within the Zijinshan Cu-Au and Luoboling Cu-Mo deposits were originally thought to reflect metal zoning resulting from hydrothermal precipitation in a porphyry-epithermal system (e.g. Li and Jiang 2017). However, our new geo-chronological data indicate that these two deposits formed during distinct hydrothermal events. It means that their contrasting metal associations reflect different magmatic processes.

Magmatic-hydrothermal deposits have variable metal associations and Cu/Au ratios (eg. Halter et al. 2002; Richards 2011) that are controlled by the nature of the sources of magmas associated with the deposits. For example, the mantle contains higher concentrations of Cu (145 ppm; Gill, 1981) and Au (Rudnick and Gao 2003) than the bulk continental crust (Cu = 27 ppm; Rudnick and Gao 2003), whereas the majority of Mo is derived from continental crustal sources (eg. Klemm et al. 2008). This means that magmas derived from different sources are usually associated with mineral deposits with different metal compositions (e.g. Richards 2011). In addition, magmatic processes might also affect the metal associations and metal ratios within mineral deposits (e.g. Halter et al. 2002). Residual sulfide phases in sources or magma could affect the Cu/Au ratios of porphyry deposits because the partition coefficients for Au partitioning into sulfide phases relative to silicate melts ($D_{(Au)}^{sulfide/silicate\ melt}$ = 2000-20,000, Li and Audétat 2013) are larger than those for both Cu ($D_{(Cu)}^{sulfide/silicate\ melt}$ = 550-10,000; Jugo et al. 1999; Halter et al. 2002) and Mo ($D_{(Mo)}^{sulfide/silicate\ melt}$ = 15-200, Li and Audétat 2012). However, the Cretaceous magmatism recorded within the ZOF is highly oxidized (eg. Xu et al. 2017), which could have suppressed the fractionation of sulfide during the evolution of magmas within this system. Consequently, the different metal associations within the Zijinshan and Luoboling deposits were possibly controlled by variations in magma source composition rather than the effect of residual sulfide phases.

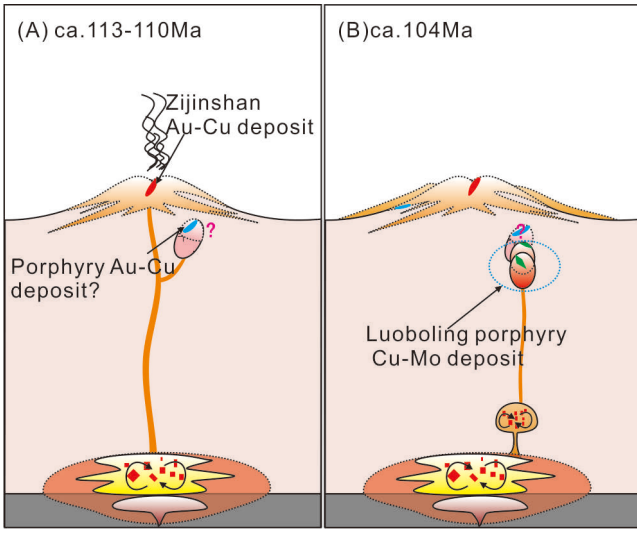

Figure 4. Schematic diagrams showing a possible model for the genesis of Cretaceous igneous rocks and related mineralization within the ZOF. (A) Mantle-derived magmas mixed with crustal material to produce Au-Cu enriched magmas that were emplaced in the ZOF at ca. 113 Ma, forming the Zijinshan HSE Au-Cu deposit. (B) Continuing crust-mantle mixing added crustal materials into the magmas in this area, eventually generating the Cu-Mo enriched magmas that were emplaced at ca. 103 Ma and formed the Luoboling porphyry Cu-Mo deposit.

The zircon $\varepsilon_{Hf}(t)$ values of the ZOF igneous rocks show a positive correlation with their zircon U-Pb ages, where crypto-explosive breccia associated with the Zijinshan HSE Au-Cu mineralization (112.9 ± 1.2 Ma) and the Luoboling granodiorite porphyry (103.8 ± 0.9 Ma) have ε_{Hf} (t) values of -1.5 to -0.5 and -4.5 to -1.2, respectively. The ca. 103 Ma magmas associated with the porphyry Cu-Mo

mineralization were most likely derived from a source containing more crustal material (Fig. 4B) than the ca. 110 Ma magmas associated with the epithermal Au-Cu mineralization in the ZOF (Fig. 4A). These distinct source variations could be a controlling factor on the different metal associations present within the adjacent HSE Au-Cu and porphyry Cu-Mo deposits in the ZOF.

Acknowledgements

This work was financially supported by the Natural Science Foundation of China (grants 41502073 and 41772065) and the National Key R&D Program of China (grant 2016YFC0600407).

References

Arribas A, Hedenquist JW, Itaya T, Okada T, Concepcion RA, Garcia JS (1995) Contemporaneous Formation of Adjacent Porphyry and Epithermal Cu-Au Deposits over 300 Ka in Northern Luzon, Philippines. Geology 23:337-340.

Cardon O, Reisberg L, Andre-Mayer AS, Leroy J, Milu V, Zimmermann C (2008) Re-Os systematics of pyrite from the bolcana porphyry copper deposit, apuseni mountains, Romania. Economic Geology 103(8):1695-1702.

Chen HS (1996) The research on the mineralization chronology and isotopic exploration assessment for Zijinshan copper-gold deposit: Geotectonica et Metallogenia. 20:343-350.

Deyell C, Hedenquist J (2011) Trace element geochemistry of enargite in the Mankayan district, Philippines. Economic Geology 106:1465-1478.

Gill JB (1981) Orogenic Andesites and Plate Tectonics. Springer-Verlag, New York.

Halter WE, Pettke T, Heinrich CA (2002) The origin of Cu/Au ratios in porphyry-type ore deposits. Science 296:1844-1846.

Hames WE, Bowring SA (1994) An Empirical-evaluation of the argon diffusion geometry in muscovite. Earth and Planetary Science Letters 124:161-167.

Hedenquist JW, Lowenstern JB (1994) The Role of magmas in the formation of hydrothermal ore-deposits. Nature 370:519-527.

Heinrich CA, Gunther D, Audetat A, Ulrich T, Frischknecht R (1999) Metal fractionation between magmatic brine and vapor, determined by microanalysis of fluid inclusions. Geology 27: 755-758.

Heinrich CA, Driesner T, Stefansson A, Seward TM (2004) Magmatic vapor contraction and the transport of gold from the porphyry environment to epithermal ore deposits. Geology 32: 761-764.

Hemley JJ, Hunt JP (1992) Hydrothermal ore-forming processes in the light of studies in rock-buffered systems some general geologic applications. Economic Geology 87:23-43.

Huang WT, Li J, Liang HY, Wang CL, Lin SP, Wang XZ (2013) Zircon LA-ICP-MS U-Pb ages and highly oxidized features of magma associated with Luoboling porphyry Cu-Mo deposit in Zijinshan ore field, Fujian Province: Acta Petrologica Sinica 29:283-293.

Jiang SH, Liang QL, Bagas L, Wang SH, Nie FJ, Liu YF (2013) Geodynamic setting of the Zijinshan porphyry-epithermal Cu-Au-Mo-Ag ore system, SW Fujian Province, China: Constrains from the geochronology and geochemistry of the igneous rocks. Ore Geology Reviews 53:287-305.

Jiang SH, Bagas L, Liang QL (2017) Pyrite Re-Os isotope systematics at the Zijinshan deposit of SW Fujian, China: Constraints on the timing and source of Cu-Au mineralization. Ore Geology Reviews 80:612-622.

Jugo PJ, Candela PA, Peccoli PM (1999) Magmatic sulfides and Au:Cu ratios in porphyry deposits: an experimental study of copper and gold partitioning at 850°C, 100MPa in a haplogranitic melt-pyrrhotite-intermediate solid solution-gold metal assemblage, at gas saturation. Lithos 46:573-589.

Klemm LM, Pettke T, Heinrich CA (2008) Fluid and source magma evolution of the Questa porphyry Mo deposit, New Mexico, USA. Mineralium Deposita 43:533-552.

Kirschner DL, Cosca MA, Masson H, Hunziker JC (1996) Staircase Ar40/Ar39 spectra of fine-grained-white mica: Timing and duration of deformation and empirical constraints on argon diffusion. Geology 24:747-750.

Li B, Jiang SY (2017) Genesis of the giant Zijinshan epithermal Cu-Au and Luoboling porphyry deposits in the Zijinshan ore district, Fujian Province, SE China: A multi-isotope and trace element inverstigation. Ore Geology Reviews 88:753-767.

Li Y, Audétat A (2012) Partitioning of V, Mn, Co, Ni, Cu, Zn, As, Mo, Ag, Sn, Sb, W, Au, Pb, and Bi between sulfide phases and hydrous basanite melt at upper mantle conditions. Earth & Planetary Science Letters 355-356:327-340.

Mao JR, Tao KY, Lee JY, Xie FG, Xu NZ (2002) Geochronology and geochemical characteristics in late Mesozoic Sifang pluton, southwestern Fujian, and their significanc. Acta Petrologica Sinica 18(4):449-458.

Renne PR, Cassata WS, Morgan LE (2009) The isotopic composition of atmospheric argon and Ar^{40}/Ar^{39} geochronology: Time for a change? Quaternary Geochronology 4:288-298.

Richards JP (2011) Magmatic to hydrothermal metal fluxes in convergent and collided margins. Ore Geology Reviews 40:1-26

Rudnick RL, Gao S (2003) Composition of the continental crust. In: Rudnick, R.L. (Ed.), Treatise on Geochemistry 3: The Crust. Elsevier, Amsterdam.

Seedorff E, Barton MD, Stavast WJA, Maher DJ (2008) Root Zones of Porphyry Systems: Extending the Porphyry Model to Depth. Economic Geology 103:939-956.

Snee LW (2002) Argon thermochronology of mineral deposits; a review of analytical methods, formulations, and selected applications, In: 2194, U.S.G.S.B. (Ed.).

So C, Zhang DQ, Yun ST, Li DX (1998) Alteration-mineralization zoning and fluid inclusions of the high sulfidation epithermal Cu-Au mineralization at Zijinshan, Fujian Province, China. Economic Geology 93:961-980.

Xu C, Chen H, Huang W, Qi J, Duan G, Zhang L, Wu C, Zhang S, Zhong W (2017) Mesozoic multiphase magmatism at the Xinan Cu–Mo ore deposit (Zijinshan Orefield): Geodynamic setting and metallogenic implications. Ore Geology Reviews 88:768-790.

Zhang DQ, Li DX, Feng CY, Dong YJ (2001) The Temporal and Spatial Framework of the Mesozoic Magmatic System in Zijinshan Area and Its Geological Significance. Acta geologica Sinica 22:403-408.

Zhang DQ, Feng CY, Li DX, She HQ, Dong YJ (2005) The evolution of ore-forming fluids in the porphyry-epithermal metallogenic system of Zijinshan area. Acta Geoscientica Sinica 26:127-136.

Zhang JJ (2013) Geology, exploration model and practice of Zijinshan ore concentrated area. Mineral Deposits 32:757-766.

Zhong J, Chen YJ, Pirajno F, Chen J, Li J, Qi JP, Li, N (2014) Geology, geochronology, fluid inclusion and H-O isotope geochemistry of the Luoboling Porphyry Cu-Mo deposit, Zijinshan Orefield, Fujian Province, China. Ore Geology Reviews 57:61-77.

Zhou S, Chen HS (1996) Geochronology and geological significance of the Zijinshan copper-gold deposit. Bulletin of Mineralogy. Petrology and Geochemistry 15:216-219.

Mineralogical and geochemical evidence of late epithermal alteration in the Kışladağ porphyry gold deposit, Uşak, Western Turkey

Ömer Bozkaya, Gülcan Bozkaya
Pamukkale University, Turkey

Nurullah Hanilçi, Davut Laçin
Istanbul-Cerrahpaşa University, Turkey

David A. Banks
University of Leeds, United Kingdom

I. Tonguc Uysal
Australian Resources Research Center (ARRC), CSIRO, Australia

Abstract. The Kışladağ porphyry gold deposit is related to Miocene intrusive and sub-volcanic rocks that resulted from an extensional tectonic regime in western Anatolia. The main lithologies of the deposit are quartz-trachytes to quartz-latites and volcanoclastic rocks intruded by sub-volcanic porphyritic rocks. Three different intrusive phases which have been identified from their age, alteration grade and mineralization (IN-1: the oldest intrusion, intense potassic alteration, IN-2/2A: intense clay-quartz alteration, IN-3: the youngest intrusion, weak alteration). IN-1 contains quartz, illite and kaolinite, IN-2A has quartz, adularia, illite, kaolinite and smectite. Alunite, jarosite and tourmaline increase in IN-1 and IN-2A; whereas biotite and illite increase in IN-1 and IN-2A, respectively. The volcanoclastic rocks are composed of quartz, alunite and kaolinite/halloysite indicating advanced argillic alteration. Although the microscopic data confirms potassic and phyllic alterations in IN-1 and IN-2A, mineralogical (well crystallized 1*M* and poorly crystallized 1M_d illite, kaolinite/halloysite, alunite, jarosite) and geochemical (K/Ar age data for different grain-sized illite indicating late overprinting at least 5 Ma) data indicate that the early stage alteration phases were overprinted by the late stage epithermal alteration.

1 Introduction

The Kışladağ Au deposit is Europe's largest porphyry type deposit (approximately 535.4 million tonnes total Au ore, 13 tonnes gold production per year, *https://www.tuprag.com.tr*) situated in western Turkey. The Kışladağ Au deposit is related to intrusive and sub-volcanic rocks of the Beydağı volcanic complex (17.3 to 12.2 Ma), resulting from extensional tectonics in western Anatolia (Figure 1; Karaoglu and Helvacı 2012). The main lithologies of the deposit area are quartz-trachyte to quartz-latite flows and volcanoclastic rocks that were intruded by a series of nested sub-volcanic alkali porphyritic intrusives (Figure 2; Juras et al. 2010; Baker et al. 2016).

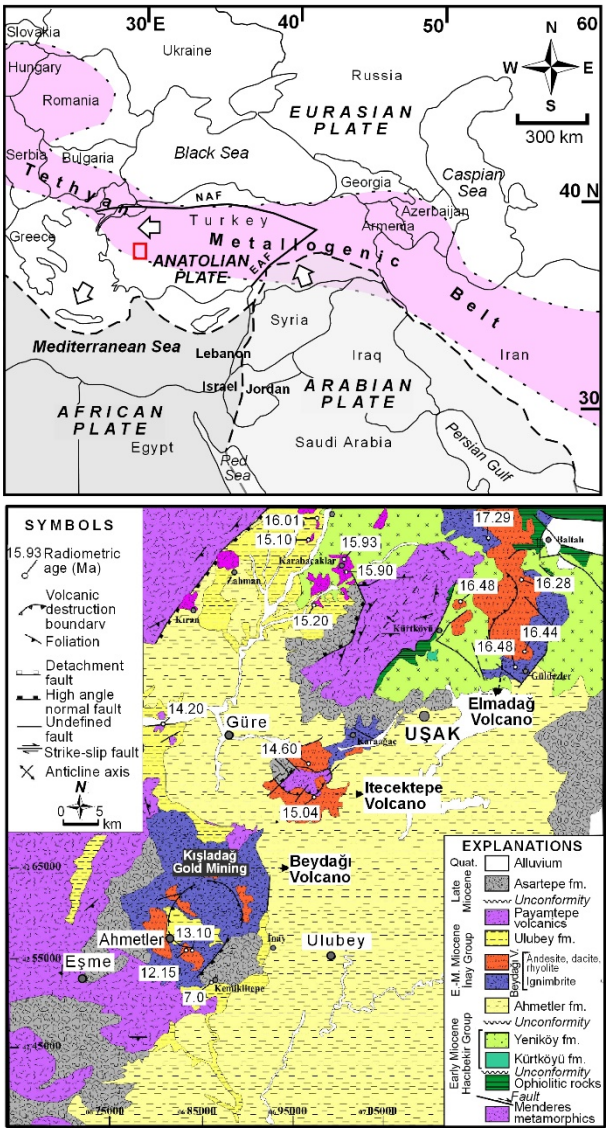

Figure 1. Location of the Kışladağ gold deposit in relation to the boundaries of Tethyan Metallogenic Belt (Yiğit 2012) and geological map of the Uşak area (Karaoğlu and Helvacı 2012).

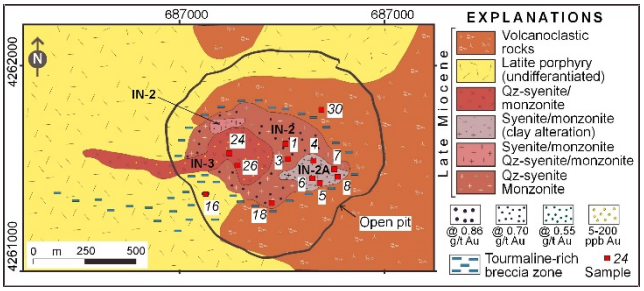

Figure 2. Geology map of the Kışladağ gold deposit (modified from Juras et al. 2010 and Baker et al. 2016).

The intrusions have a monzonitic character based on their mineralogy and chemistry and they have been sub-divided according to cross-cutting relationships, alteration and mineralization as (i) intrusion 1 (IN-1), (ii) intrusion 2 (IN-2) and the altered equivalent of intrusion 2 (IN-2A), (iii) intrusion-3 (IN-3) (Baker et al. 2016). Gold mineralization occurs within the IN-1, IN-2 and IN-2A. Intrusive rocks which were intruded into the basement metamorphic rocks and overlain by Miocene volcanics.In this study, we have investigated late epithermal (argillic) alteration that overprints the initial potassic and phyllic (sericitic) alteration related to the porphyry system. Thus, it may be possible to evaluate the alteration mineralogy in combination with new radiogenic isotope data from clay and alunite from the alteration zones.

2 Geological Setting

The Kışladağ porphyry gold deposit is located in western Anatolia within the extension-related Neogene Uşak-Güre basin (Figure 1). The NE-SW-trending Uşak-Güre basin formed upon the Menderes metamorphic basement which was exhumed during extension (Karaoğlu et al. 2010). Basement units of the massif include augen gneisses, schist, and marble, and the structurally overlying Upper Cretaceous ophiolitic mélange rocks. The Kışladağ Au deposit occurs mainly within the intrusive rocks of the eroded Miocene Beydağı stratovolcano. Three different phases of intrusions (IN-1 to 3) have been identified from their cross-cutting relationships, alteration and mineralization (Figure 2, Baker et al. 2016). IN-1 is the oldest and best mineralized (0.86 g/t Au) intrusive phase and forms the core of the system. Alteration samples from IN-1 are characterized by tourmaline bearing quartz veins and fine-grained (sericitic) biotites (Figure 3a). IN-2 is a fine to medium-grained porphyritic rock, with intense pervasive clay-quartz alteration in IN-2A (Figure 3b) IN-2A samples (0.55 g/t Au) are characterized by an abundance of fine-grained (sericitic) white K-mica (illite) and completely sericitized feldspar phenocrysts. Intrusion IN-3, the youngest intrusive body (<5 to 200 ppb Au), is a fine-grained porphyritic rock and contains unaltered plagioclase, with rare quartz and biotite phenocrysts. The volcanoclastic rocks cover a wide area and show fine grained fragmental ash fall tuffs with pumice fragments and porphyritic flows.

3 Results

3.1 Optical Microscopy

Photomicrographs of the main alteration textures are shown in Figure 3. Feldspar phenocrysts are replaced by kaolinite in altered sub-volcanic rocks IN-1 and IN-2A which retains a primary porphyritic texture (Figure 3a, b). Kaolinites were developed replacing feldspars and also infilling pore spaces and cracks. Alunites are present as euhedral to subhedral prismatic crystal aggregates in alunite-bearing quartz veins (Figure 3c). In strongly silicified volcanoclastic rocks, a primary pyroclastic (vitroclastic) texture is evident and most of the samples are composed of hydrothermal quartz and partly pore-filling kaolinite. The textural evidence indicates that the advanced argillic alteration overprints the initial potassic and sericitic alteration.

3.2 Scanning Electron Microscopy

Scanning electron microscope data of altered samples from IN-1 show that fine-grained (<2 μm) illites are distinguished from coarse grained tabular illite/mica stacks (Figure 4a). Acicular rod-like adularia crystals are associated with flaky/tabular illites and coin-shaped alumina-silica phases in highly altered porphyry rocks from IN-2A (Figure 4b). Euhedral adularia crystals are found as formerly occurred phase and jarosite, illite and smectite crystals were subsequently developed as low-temperature phases (Figure 4c-d). The co-existence of fine and coarse grained (mica-like) platy illites indicate late epithermal (argillic) alteration overprinting the earlier phyllic and potassic alteration. In addition to this overprinting, the development of alunite and halloysite (Figure 4e-f) in highly silicified volcanoclastics from the outer parts of ore deposit, indicate a separate phase of argillic alteration.

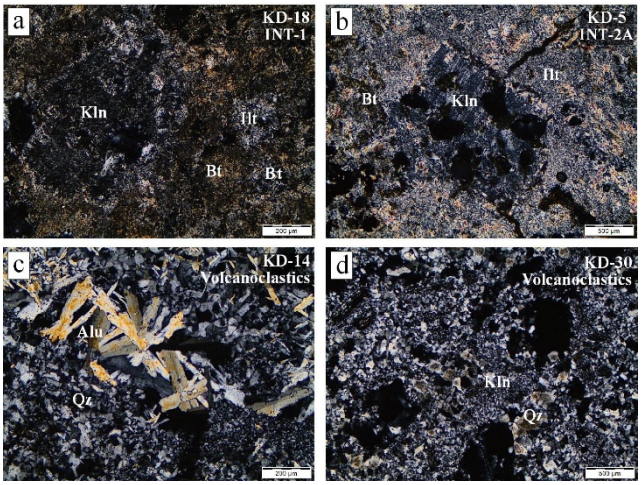

Figure 3. Optical microscopic photomicrographs of hydrothermally altered samples (crossed nicols) (a-b) Fine-grained (sericitic) biotite and white mica (illite) in the matrix, with kaolinites replacing feldspars in altered porphyry rock from IN-1 and IN-2A, (c) Alunite crystals in quartz veins in volcanoclastics, (d) Primary pyroclastic (vitroclastic) texture of silicified volcanoclastic rocks with pore-filling kaolinite.

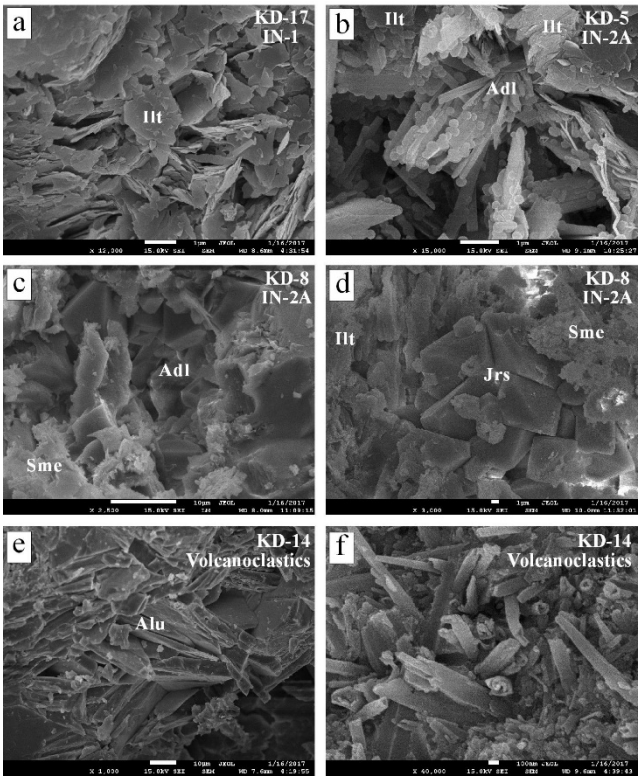

Figure 4. Scanning electron microscope photomicrographs of hydrothermally altered samples (a) Coarse- and fine-grained flaky illites, (b) Acicular rod-like adularia crystals associated with flaky/tabular illites, (c) Euhedral adularia crystals and plumy smectites, (d) Euhedral jarosite crystals together with flaky illite and plumy smectite, (e) Tabular/platy alunite crystals, (f) Tubular halloysite crystals in silicified volcanoclastic rocks.

3.3 X-ray Diffraction

Whole rock and clay fraction mineralogical compositions of the altered samples, obtained using a GNS APD 2000 X-ray diffractometer, are given in Table 1 and Figure 5. Quartz and feldspar (plagioclase) are the main minerals in almost all samples, Clay minerals are illite, kaolinite and smectite. The main clay mineral assemblage is illite + kaolinite ± smectite.

Table 1. X-ray diffraction whole-rock and clay fraction mineral composition of the samples from alteration zones (+: 20%, ± <5%). Qz: Quartz, Fsp: Feldspar, Alu: Alunite, Jrs: Jarosite, Fs: Phyllosilicate, Sme: Smectite, Kln: Kaolinite, Ilt: Illite, Chl: Chlorite.

Sample No	Whole Rock				Clay Fraction (<2μm)				KI (Δ°2θ)	I_{002}/I_{001}
	Qz	Fsp	Alu/Jrs	Fs	Ilt	Kln	Sme	Chl		
Intrusive 1 (IN-1)										
KD-3	++			+++	++	+++				
KD-17	++	Jrs±	Alu±	+++	+++++				0.54	0.31
KD-18	++			+++	++++	+			0.53	0.40
Intrusive 2A (IN-2A)										
KD-4	++	±		+++	++	+++			0.62	0.48
KD-5	++	±	Alu±	+++	++++	+			0.68	0.45
KD-6	+	+		+++	++	+	++		0.45	0.51
KD-7	+	+		+++	++++	+		±	0.55	0.62
KD-8	+	+	Jrs±	+++	+	+	+++		0.42	0.56
Volcanoclastic rocks										
KD-13	+	+		+++	+++	++			0.50	0.51
KD-14	++		Alu ++	+	+++	++			-	-
KD-30	++++	±		+		+++++			-	-

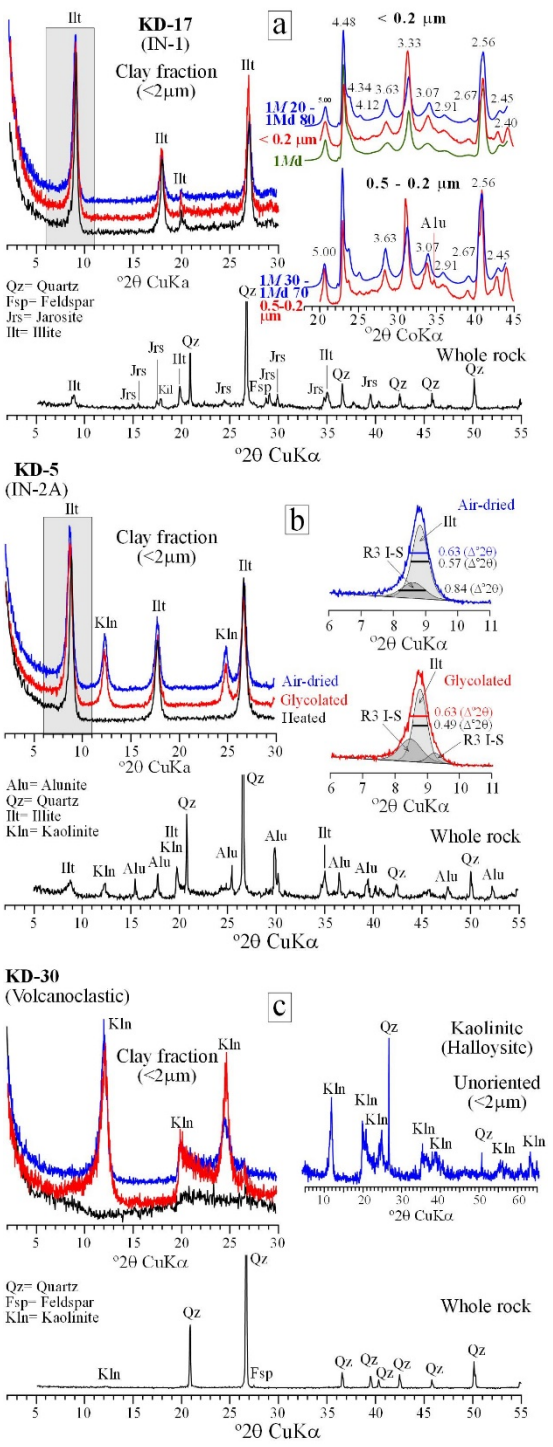

Figure 5. X-ray diffraction patterns of whole rock and clay fractions from different alteration zones.

Polytype data for illites of different grain-sizes, show that 1*M* illite is related with the coarse-grained size fraction (i.e. phyllic or potassic alteration stage), whereas 1*M*d illite is associated with the fine-grained fraction (i.e. late stage epithermal stage) (Figure 5a). The 10 Å illite peak decomposition data indicates that two types of illitic phases (well crystallized illite and poorly crystallized illite or R3 I-S) are present (Figure 5b). This data also confirms a late epithermal overprint.

3.4 Mineral chemistry and K/Ar age of illites

SEM-EDS analysis of illite/micas, evaluated on Si - Na+K and M^+ - 4Si - R^{2+} diagrams, indicate compositions between muscovite-phengite-illite (Figure 6). The wide range of illite/mica compositions results from different grain sized illitic phases, resulting from different origins (i.e. muscovite-phengite for the phyllic stage and illite for argillic stage).

K/Ar age data of different grain-size illites and one alunite, analysed at the CSIRO isotope laboratory, Australia, is given in Table 2 and Figure 7. K/Ar age data changes for different grain-sizes, the larger sizes, 2-0.5 µm and 0.5 to 0.2 µm are always older than the smallest size fraction, i.e. 17-15 Ma for 0.5-0.2 µm grain size, whereas 14-13 Ma for <0.2 µm. The age of alunite from volcanoclastic rocks has been determined as 17.6±0.5 Ma. Our illite and alunite age data correlate with the literature data (age of host rocks and hydrothermal mineralization), the ages of coarse-grained illites are older than argillic alteration (Figure 7). This means coarser grains contain phyllic alteration related illitic phases because of the relatively higher temperature related occurrences. Two samples (KD-14 alunite and KD-17 illite 0.5-0.2 µm) have an older age and therefore they should be omitted for the evaluation. The younger ages for the fine grain size (<0.2 µm) illites represent a later and/or much younger thermal event and thus confirm the argillic alteration overprint of the potassic and sericitic/phyllic alterations (Figure 7).

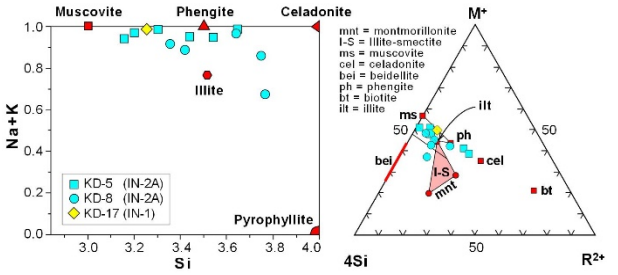

Figure 6. Distribution of illite/mica compositions on Si - Na+K and M^+ - 4Si – R^{2+} diagrams.

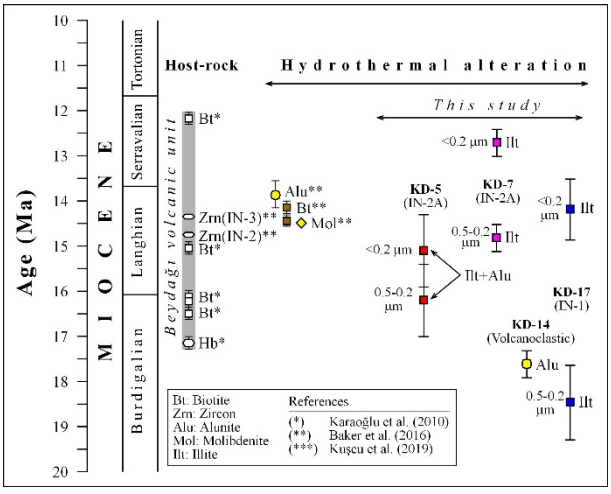

Figure 7. Chronological distribution of K/Ar age data from different sized illites and alunite.

Table 2. K/Ar ages of different size illites and alunite.

Sample	Mineral	Lithology	Size (µm)	K (%)	Ar (%)	Age (Ma)
KD-17	Illite	IN-1 porphyry	<0.2	6.54	7.2	14.2±0.9
KD-17	Illite		0.5-0.2	5.97	4.4	18.5±1.8
KD-17	Illite		2-0.5	5.24	2.3	18.9±3.3
KD-5	Illite	IN-2A porphyry	<0.2	5.03	2.9	15.1±2.1
KD-5	Illite		0.5-0.2	4.94	3.4	16.2±2.1
KD-5	Illite		2-0.5	4.88	4.7	15.8±1.4
KD-7	Illite	IN-2A porphyry	<0.2	5.91	36.7	12.7±0.3
KD-7	Illite		0.5-0.2	6.12	56.8	14.8±0.4
KD-7	Illite		2-0.5	6.36	57.0	14.5±0.3
KD-14	Alunite	V.clastic	<2.0	5.49	27.2	17.6±0.5

4 Discussion and Conclusion

Three different intrusive phases are present in the Kisladag deposit, each showing different types of alteration. IN-1, the oldest intrusion, is associated with intense potassic alteration, IN-2/2A, with intense clay-quartz alteration and IN-3, the youngest intrusion, is only weakly altered. Although the data confirms potassic and phyllic alterations in IN-1 and IN-2A, mineralogical (well crystallized 1M and poorly crystallized 1Md illite, kaolinite/halloysite, alunite, jarosite) and K/Ar ages indicate that the early stage alteration phases were overprinted by the later, much younger, epithermal alteration. Illite peak decomposition (well crystallized and poorly crystallized illites) and illite polytype data (1*M* illite for coarse-grains, 1*M*d illite for fine-grains), clearly indicate two different stages of alteration. Different types of illitic phases, well crystallized illite and poorly crystallized illite or R3 I-S, are found (Figure 5b).

The wide range of illite compositions and K/Ar ages confirm this interpretation. K/Ar dating of different grain-sizes of illites and alunite indicate that the epithermal overprint started shortly after the potassic and sericitic/phyllic alteration of the porphyry system. This shows the duration of hydrothermal activity and mineralization at Kisladag was at least 5 Ma.

References

Baker T, Bickford D, Juras S, Lewis P, Oztas Y, Ross K, Tukac A, Rabayrol F, Miskovic A, Friedman R, Creaser RA, Spikings R (2016) The Geology of the Kışladağ Porphyry Gold Deposit, Turkey. Society of Economic Geologists, Inc. Special Publication 19: 57-83

Juras S, Miller R, Skayman P (2010) Technical Report for the Kışladağ Gold Mine, Turkey, Eldorado Gold Mining.

Karaoğlu Ö, Helvacı C (2012) Structural evolution of the Uşak-Güre supra-detachment basin during Miocene extensional denudation in western Turkey. J Geol Soc 169: 627-642

Karaoğlu Ö, Helvacı C, Ersoy EY (2010) Petrogenesis and $^{40}Ar/^{39}Ar$ geochronology of the volcanic rocks of the Uşak-Güre basin, western Türkiye. Lithos 119: 193-210

Kuşcu I, Tosdal RM, Gencalioğlu-Kuşcu G (2019) Episodic porphyry Cu (-Mo-Au) formation and associated magmatic evolution in Turkish Tethyan collage. Ore Geol Rev 107: 119-154

Yiğit Ö (2012) A prospective sector in the Tethyan Metallogenic Belt: geology and geochronology of mineral deposits in the Biga Peninsula, NW Turkey. Ore Geol Rev 46:118-148

Au-Ag-Te and Au-Ag-Se mineralizations as indicators of high- low sulfidation types of epithermal deposits of the Kurama volcanic-plutonic region (Uzbekistan)

Rustam Khalmatov,
Centre for Advanced Technologies

Rustam Koneev
National University of Uzbekistan, Tashkent, Uzbekistan

Margarita Kim
Institute of Geology and Geophysics, Tashkent, Uzbekistan

Abstract. Geochemical and micro-nanomineralogical methods have been used to study the high sulfidation ores of the Kochbulak deposit and low sulfidation ores of Kyzylalmasay. The high sulfidation type is defined as Au-Ag-Te, gold-telluride-polymetallic, and low sulfidation Au-Ag-Se, electrum-selenide-sulfosalt. Such an approach enhances the capabilities of geochemical and mineralogical and geochemical methods in the search for, classification and evaluation of hidden gold mineralization.

1 Introduction

Current researchers of the epithermal deposits of volcanogenic regions mainly follow the classification of J. Hedenquist et al. (1996). Two types of deposits are distinguished; High and Low sulfidation (HS and LS) differing in the composition of nonmetallic minerals: alunite, barite (HS), and sericite, adularia (LS). In the study of industrial deposits, the main focus should be on gold and ore elements (Te, Se, Ag, As, Sb, Bi, Hg), which determine its geochemistry, mineralogy and metallogeny. Gold compounds with the listed elements usually belong to rare, secondary ones however, in terms of frequency of occurrence and content in ores, they are not inferior and even exceed gold – the main economically valuable component. During the enrichment of ores, gold is extracted from concentrates of ore minerals. Nonmetallic – quartz, carbonates, feldspars, mica and others are waste products of enrichment and more often have a negative effect on gold recovery.

The purpose of research is the study of gold, related elements and minerals, to understand the genesis, develop search criteria, classify and evaluate new hidden deposits.

2 Methods

Polished thin sections and polystyrene briquettes with pressed concentrates have been studied. The studies were conducted on an Electron microprobe JXA Superprobe 8800R and a Zeiss electron microscope EVO/MA 10 (SEM-EDX). Geochemical analysis was performed on an Agilent Technologies ICP MS 7500 mass spectrometer. Considering that gold in primary sulfide ores is a typical micro-nanomineral (size from 100 to 0.00n μm), micro-nanomineralogical research methods have been applied (Koneev et al. 2010).

3 Geology

The Kurama region is the Eastern end of the Valeriano-Beltau-Kurama volcano-plutonic arc. Andesite volcanism and granitoid plutonism are commonly present in the region. The age of super-subduction magmatism is 320–289 Ma (U-Pb, SHRIMP), the age of epithermal pyrite mineralization is 298 Ma (Os-Re) (Dolgopolova et al. 2017). For comparative studies, two reference representatives of epithermal deposits were selected – HS type Kochbulak field and LS type Kyzylmalmasay field. On Kochbulak, ore bodies are represented by steeply dipping veins, interfacial vein-metasomatic deposits, pipes of explosive breccia with gold content up to 20 000 g/t (Fig. 2 A). They are placed in berezitized and argilized dacites and andesites (C_2), in sub-latitudinal and sub-meridional faults (Fig. 1 I). At Kyzylalmasay, ore bodies are represented by veins, interformational lodes in argilized and berezitized andesites, syenite-diorites (C_2), granites (S_2-D_1) with a block of chlorite-sericite schist xenoliths (Fig. 2 B). The ore-enclosing structure is the 10 km-long Main ore-bearing zone formed by the Kyzylalmasay and Karabausky faults (Fig. 1 II).

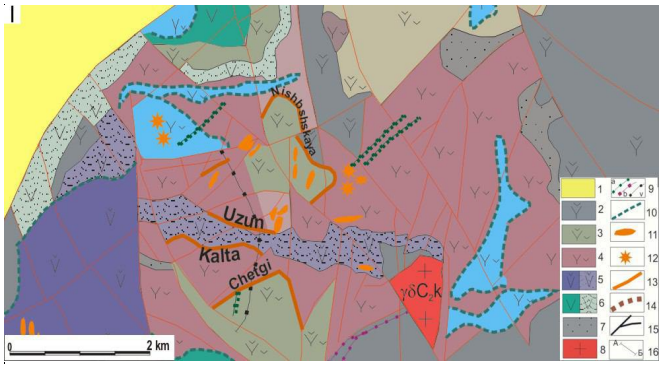

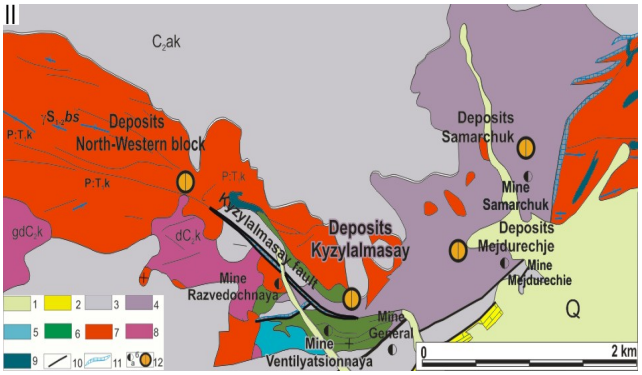

Figure 1. Geological map of Kochbulak (I) and Kyzylalmasay (II) ore fields (Atlas, 2010).
I- Kochbulak:1 - Mesozoic-Cenozoic formations; 2-trachyandesite; 3-trachyandesidacites; 4-andesites; 5-trachyandesites; 6-dacites; 7-volcanomictous sandstones, gritstones; 8 - granitoids; 9 - dikes: diabase a) porphyrites, b) felsites, v) granosyenite-porpyrites; 10 - subvolcanic bodies; 11-vein and metasomatic; 12-tubular ore bodies; 13-gentle mineralization zones; 14-Kochbulak caldera; 15 –fractures.
II-Kyzylalmasay: 1.Quaternary deposits; 2. Cenozoic deposits; 3.Akcha complex; 4.Bolgala complex; 5.Subvolcanic facies of Bolgala complex; 6.Early Paleozoic shales; 7.Bashkyzylsay granitoid complex; 8.Karamazar granit-adamellite complex; 9.Dikes of syenite-diorites; 10.Dikes felsites; 11.Quartz velns; 12.Mines (a) and areas of deposit (b).

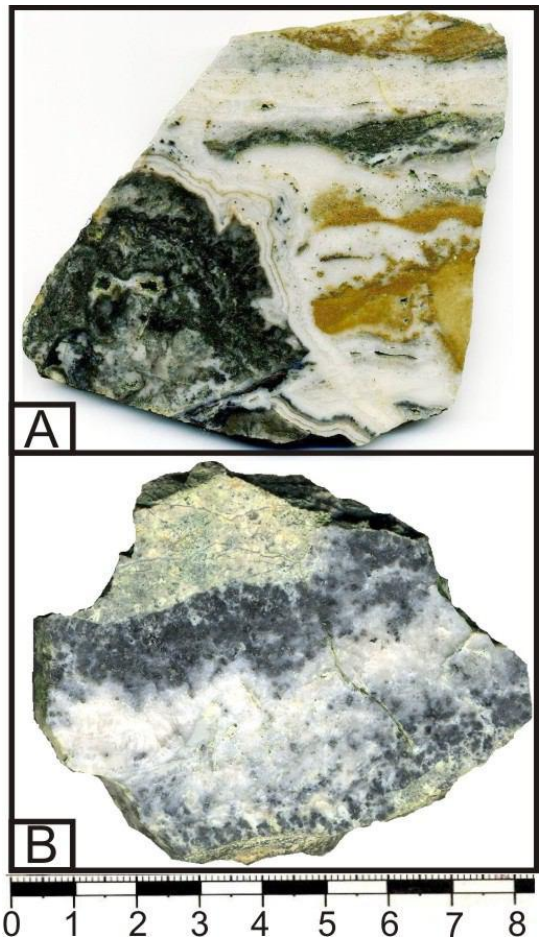

Figure 2. Samples of ores with Au-Ag-Te and Au-Ag-Se mineralization. A – Kochbulak; B – Kyzylalmasay.

4 Research results

Quartz, calcite, feldspars, alunite barite, pyrite, tetrahedrite, galena, sphalerite, chalcopyrite, bismuthinite dominate in ores of the Kochbulak deposit. The ratio Au:Ag is 10:1-1:10, Se:Te is 1:1-1:30. Geochemical leaders are Te, Au, Bi, Sb, Ag, Se, Cu, Pb (Kovalenker et al. 1997; Khalmatov et al. 2015) Micro-nanomineralogical studies have established a wide distribution of various tellurides, especially Au and Ag (Table 1). Gold has high fineness (800–1000‰). The relationship of gold and tellurides with matrix minerals is shown in figure 3, I.

Ores of the Kyzylalmasay deposit are represented by quartz, ankerite, sericite, adularia, pyrite, chalcopyrite, freibergite, acanthite (Khalmatov 2009). The ratio Au:Ag – 1:10-1:100, Se:Te – 10:1-1:10. Geochemical leaders are Ag, Au, Sb, Se, Cu, Te. A wide distribution in the upper and middle horizons of selenides were established (Table 1). The relationship of selenides and other Ag minerals are shown in figure. 3, II. At deep levels, the concentration of Te, Bi, Pb and the corresponding compounds increases. Gold is represented by electrum, custelite and petrovskaite (AuAgS). The standard of 750 to 450‰ increases with depth. Silver in various minerals is often marked with Se impurity (0,n-2%).

On Kochbulak and Kyzylalmasay, except Au-Ag-Te and Au-Ag-Se types manifested early identical for both deposits Au-As, quartz-pyrite-arsenopyrite association, which occupies the bulk of the ore bodies. The gold is predominantly fine in there. Nickel minerals – gersdorffite, loellingite are also characteristic.

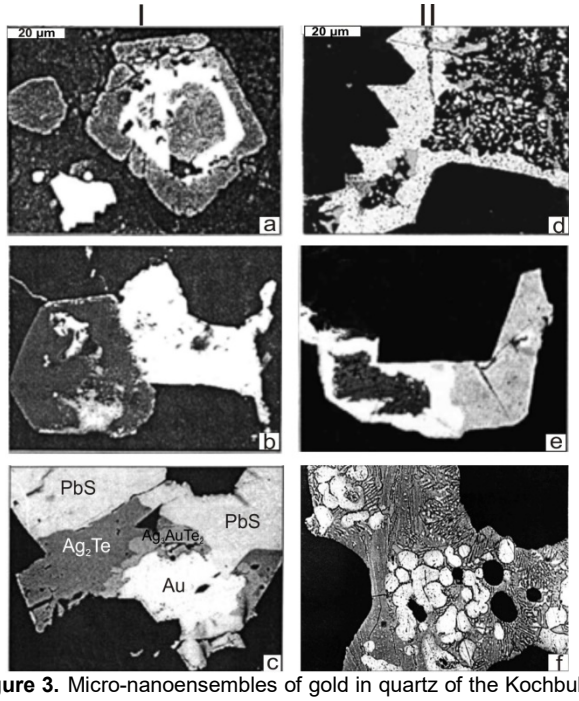

Figure 3. Micro-nanoensembles of gold in quartz of the Kochbulak deposit (I) and an ankerite of the Kyzylalmasai deposit (II). I-row: a - goldfield and gold in the areas of growth of pyrite, b - replacement of pyrite with gold tellurides, c - gold, Hessite, petzite and galena; II-row: e - selenides, silver-bordered sulfosalts, f - silver-bordered Naumanite and Bogdanovichite rims around pyrite, g - silver, selenides, sulfosalts in freibergite.

Table 1. Chemical composition of tellurides and selenides in the epithermal deposits (mass. %)

Mineral	Te	Se	Au	Ag	Cu	Pb	Bi	Sb	Hg	S	∑
Kochbulak											
Calaverite	55.64	0.14	43.23	0.52	0.45	-	-	-	-	-	100.06
Krennerite	58.85	-	37.09	3.79	-	-	-	-	-	-	99.73
Sylvanite	61.95	-	24.93	12.83	-	-	-	-	-	-	99.84
Petzite	32.41	-	23.28	42.48	0.95	-	-	-	-	0.52	99.68
Nagyagite	16.20	0.32	10.13	2.14	-	53.41	-	8.23	-	10.06	100.55
Altaite	37.81	-	-	-	-	61.76	-	-	-	-	99.72
Coloradoite	39.10	-	-	-	0.15	-	-	-	60.62	-	100.02
Tellurantimony	62.27	0.41	-	-	-	-	-	37.31	-	-	99.99
Tetradymite	35.56	0.63	-	0.04	-	-	59.00	0.35	-	4.42	100.00
Kyzylalmasay											
Aguilarite	-	12.45	-	80.43	0.38	-	-	-	-	6.52	99.78
	-	14.11	-	77.94	0.63	-	-	-	-	7.38	100.06
Te-naumannite	2.75	21.35	-	73.06	1.53	-	0.62	-	-	0.40	100.46
	4.16	21.15	0.16	72.26	1.50	-	0.80	-	-	0.30	100.33
Naumannite	-	25.90	-	73.63	-	-	-	-	-	-	99.60
	0.48	27.24	-	73.38	-	-	-	-	-	-	101.18
Bogdanowiczite	-	33.14	-	21.59	0.28	-	44.03	0.41	-	0.51	99.96
	-	32.04	-	21.03	0.39	-	44.24	0.46	-	1.80	99.98

5 Discussion of the results and conclusions

The studies conducted on the Kochbulak and Kyzylalmasay deposits indicate that high- and low sulfidation types contrast well enough in their geochemical and mineralogical characteristics. We define HS type as Au-Ag-Te, gold-tellurium-polymetallic type. A distinctive feature of this type is the extensive development of Au, Ag, Pb, Sb, Bi, Hg tellurides with high-grade Au. In the wider Kurama region, in addition to Kochbulak, the deposits Kayragach, Samarchuk, Kauldy can be classified as this type.

The LS type corresponds to the Au-Ag-Se, electrum-selenide-sulfosalt type with the wide development of selenides, sulfosalts like polybasite, stephanite, pyrargyrite, acanthite, allargentum, silver, electrum, custelite and sulfides of Au-Ag petrovskaite. In addition to Kyzylalmasay in the region, it includes Chadak, Arabulak, Revashte.

The definition of HS and LS types as Au-Ag-Te and Au-Ag-Se enhances the capabilities of geochemical methods of searching, classifying and estimating hidden ores. In combination with micro-nanomineralogical methods of research, they provide direct indications of the corresponding ores. Alunite barite, sericite, adularia minerals are convergent and are characteristics not only of epithermal gold deposits.

Acknowledgements

The research was supported by OT-F8-01 and IZ-0929142 grants of the Ministry of Innovation Development of the Republic of Uzbekistan.

References

Atlas of models of ore deposits of Uzbekistan (2010) State Committee of the Republic of Uzbekistan on geology and mineral resources. Tashkent, Uzbekistan. 100 p.

Dolgopolova A., Seltmann R., Konopelko D. et.al. (2017) Geodynamic evolution of the western Tien Shan, Uzbekistan: Insights from U-Pb SHRIMP geochronology and Sr-Nd-Pb-Hf isotope mapping of granitoids. Gondwana Research 47. Elsevier. 2017. P. 76-109.

Hedenguist JW., Izawa E., Arribas A., White NC (1996) Epithermal gold deposits: style, characteristics and exploration. The Society of Resource Geology. Tokyo, Japan. Special Publication #1.

Koneev R.I., Khalmatov R.A., Mun Yu.S. (2010) Nanomineralogy and nanochemistry of ores from gold deposits of Uzbekistan // Geology of ore deposits, 52(8):755-766.

Khalmatov R.A., Koneev R.I. (2015) Epithermal gold mineralization of the Kurama volcanic region of the Western Tien Shan (Uzbekistan). 13th SGA Biennial Meeting. Nancy, France. P. 307-308.

Khalmatov R. (2009) The Kyzylalmasay gold-silver deposit (Uzbekistan): micromineralogy and geochemistry of ores from deep horizons. 10th SGA Biennial Meeting. Townswill, Australia. 1:117-119.

Kovalenker V.A., Safonov Yu.G., Naumov V.B., Rusinov V.L. (1997) The epithermal gold-telluride Kochbulak field (Uzbekistan). Geology of ore deposits, 39(2):127-152.

Argillic alteration of the Mikheevskoe porphyry copper deposit (South Urals, Russia)

Oksana B. Azovskova, Mikhail Y. Rovnushkin
The Zavaritsky Institute of Geology and Geochemistry, Ural Branch of Russian Academy of Sciences (IGG UB RAS)

Olga Y. Plotinskaya
Institute of Geology of Ore Deposits, Petrography, Mineralogy and Geochemistry, Russian Academy of Sciences (IGEM RAS)

Vyacheslav A. Gemel
JSC Mikheevskiy GOK

Abstract. Geological setting and mineral composition of argillic alteration of the Mikheevskoe porphyry copper deposit have been examined. Typical argillic alteration occurs as steep-dipping zones, often associated with porphyry dikes. In the upper part of the deposit such zones have uneven lateral distribution and are classified as “loose sulphide ore” which requires a specific mineral processing treatment. Typical minerals of the argillic altered rocks are: quartz, illite/hydromica, kaolinite, chlorite, unoxidized sulphides (1-5%), often carbonates (calcite, dolomite, siderite), and low temperature bitumen of kerite range (0.1-0.5%). Argillic metasomatites of the central part of the deposit contain up to 5% of pyrophyllite. Major ore minerals are pyrite and chalcopyrite, minor ones are bornite and molybdenite. Molybdenite is characterized by quite uneven, patchy-spotted distribution of rhenium which in some point analyzes peaks at 1.72 wt%, with an average content of 0.43 wt%. Accompanying mineralization is represented by Co-Ni sulphoarsenides, Se-rich galena, and sphalerite. A distinguishing feature of argillic alteration is the presence of Au-Ag, Ag, and Pb selenides, often in association with tellurides and native gold of quite a diverse composition. Compositional variability and intensity of the accompanying mineralization is controlled by both intensity of argillic alteration and distribution of earlier alteration processes.

1 Introduction

The Mikheevskoe deposit is one of the most economically significant (Mo,Au)-Cu-porphyry in Russia. It is situated 250 km south of the city of Chelyabinsk and represents part of the Novonikolaevskii ore cluster. From the regional structural perspective this area is confined to the junction of two large structures - East- and Transuralian megazones (Grabezhev 2014; Puchkov 2010). Extensive network of faults in the area results in linear blocks with sheared east-west striking linear folds within the blocks. The geology of the area features Late Devonian volcanic and volcano-sedimentary basaltic andesite and basalt formations with terrigenous layers and small bodies of serpentinite, as well as granitoids of Ulyanovsk (Late Devonian) and Mikheevsky (Late Devonian to Eraly Carboniferous) complexes (Grabezhev and Belgorodskii 1992).

Porphyry molybdenum-copper mineralization is genetically linked to the Mikheevsky igneous complex. Re-Os age of the mineralization is 357.8±1.8 and 356.1±1.4 Ma (Tessalina and Plotinskaya 2017). Mineralization is associated with a belt of quartz-diorite and diorite dikes (mostly porphyritic) which stretches between two diorite stocks of the Mikheevsky complex (Fig. 1). There is an intensive rock alteration represented by the following main alteration types and associated ore minerals (modified after (Plotinskaya et al. 2018):

1. actinolite±epidote, with magnetite, occasionally with garnet relicts (andradite);
2. biotite+muscovite±K- feldspar (potassic alteration), with bornite and chalcopyrite;
3. chlorite+epidote+sericite (propylitisation), with pyrite or pyrite and chalcopyrite;
4. quartz+sericite (quatz-sericite or phyllic alteration), with chalcopyrite and molybdenite;
5. quartz+illite/hydromica+kaolinite (argillic alteration), predominantly with pyrite, ± chalcopyrite, bornite, molybdenite.

Most abundant are the intermediate varieties – chlorite-sericite metasomatites. Notably, carbonate (calcite, dolomite, siderite) is almost always present in altered rocks, often in the form of veinlets.

Typical argillic metasomatites can be observed in the existing open as steep-dipping zones with apparent thickness of up to 40 m or more, or series of closely located thinner zones. At the same time, there are quite frequent occurrences of weaker argillic alteration superimposed on other alteration types. In the upper section argillic metasomatites extend laterally, albeit extremely unevenly (Fig. 1). Thickness of such formations varies from 1.6 to 46 m, average thickness is 14 m. They are overlain by the weathering crust, often with a gradual boundary. As a result, they are considered as a specific ore type which requires a different mineral processing circuit (Russian Copper Company).

This study is aimed to describe mineralogical and geochemical features of argillic metasomatites from steep-dipping zones in the northern part of the deposit.

2 Sampling and analytical methods

Five sites of argillic metasomatites were sampled from the open pit; 4 sites were sampled in the northern portion of the deposit, and 1 site in the central portion of the deposit. Study was carried out in the Zavaritsky Institute of Geology and Geochemistry, Ural Branch of Russian Academy of Sciences, Yekaterinburg. Bulk mineral composition of altered rocks was studied using Shimadzu XRD-7000 X-ray diffractometer and PerkinElmer Diamond TG/DTA system (analysts: N.G. Petrishcheva, T.Ya. Gulyaeva and O.L. Galahova). Mineralogy was studied using (SEM) JSM-6390LV by Jeol with energy-dispersive detector INCA Energy 450 X-Max 80 by Oxford Instruments (analysts: S.P. Glavatskikh, I.A. Gottman, L.V. Leonova). Detailed studies of specific molybdenite and pyrite grains were carried out using a Cameca SX100 electron probe microanalyser (analyst D.A. Zamyatin). Trace element composition of typical samples of argillic metasomatites were identified using ICP-MS method by Perkin Elmer ELAN-9000.

3 Results and discussion

Steep-dipping argillic alteration zones are often associated with quartz-diorite porphyry dikes and their external contacts. Typical argillic metasomatite is a whitish, light-grey, greenish, or yellowish rock that retains all of the structural and textural features of the primary rock. At the same time, it can be easily molded by hand, and 90-95% of the volume can be washed away by water. There are occasional areas and zones of silification. Most common minerals of the argillic rock are (according to X-Ray and TG/DTA analysis): fine grained quartz, illite/hydromica, kaolinite (0-15%) and unoxidized (newly formed) sulphides (1-5%). A third of the studied samples also feature low temperature bitumen (0.1-0.5%). There are also variable quantities of chlorite. ~ 50% of samples and veinlet zones contain carbonate: calcite, to a lesser extent dolomite and siderite (up to 2-3%, occasionally more). Argillic altered rock of the central part of the deposit often contains up to 5% pyrophyllite. Major ore minerals (in descending order) are: pyrite, chalcopyrite, copper sulphides, molybdenite; Co-Ni sulphoarsenides of cobaltine-gersdorffite range are typically present. There are minor amounts of galena and sphalerite.

Pyrite is the most abundant sulfide in the argillic metasomatites. It occurs, mostly, in cubic form and cube-based combinations, with grain size of ~0.01-~0.1 mm, rarely larger. SEM study of inclusions and ingrowths on the surface of pyrite grains was carried out in order to describe ore and accompanying mineralization in more detail.

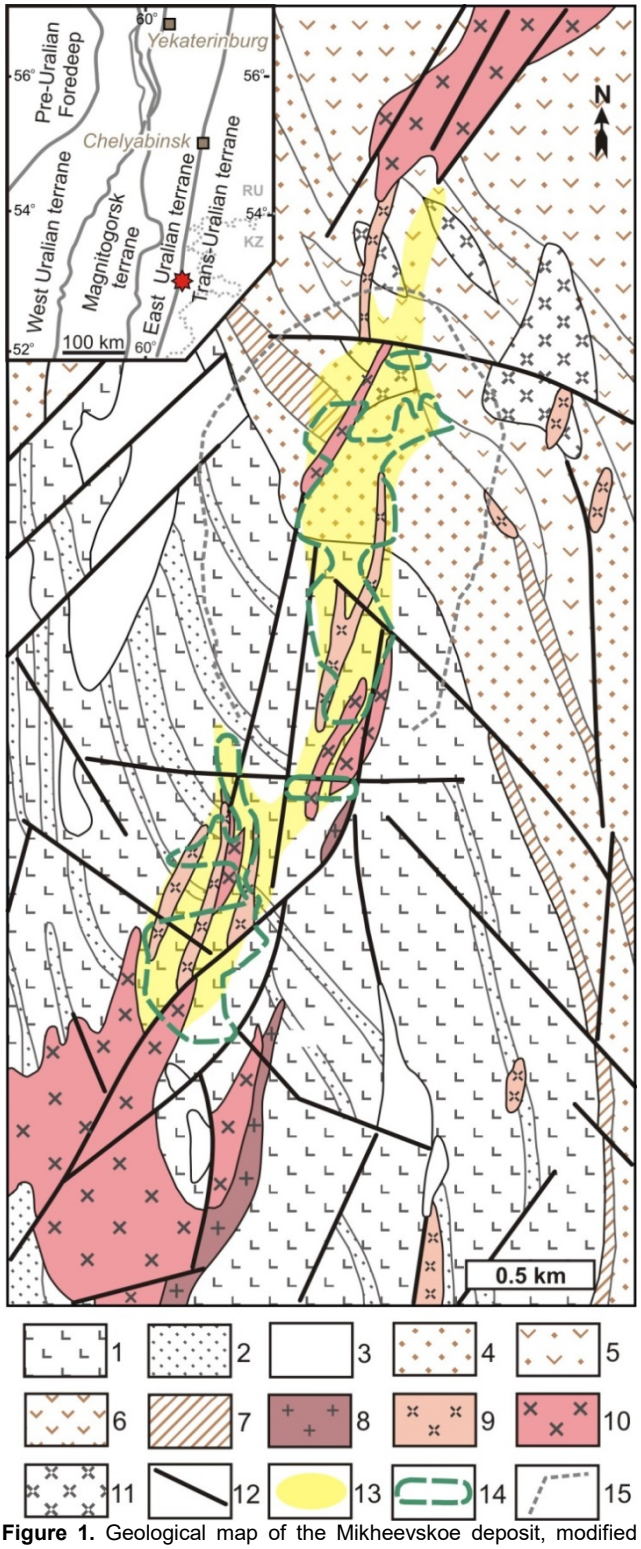

Figure 1. Geological map of the Mikheevskoe deposit, modified after (Shargorodskii et al. 2005).
Late Devonian volcano-sedimentary rocks, upper lithological unit: 1 – aphyric basalt; 2 – sandstone, chert; 3 – serpentinite; lower lithological unit: 4 – sandstone, tuffaceous sandstone; 5 – basaltic andesite volcaniclastic rock; 6 – basaltic andesite lava; 7 – quarzite, silica shale; the Mikheevsky igneous complex: 8 – plagiogranodiorite porphyry; 9 – diorite porphyry; 10 – quartz diorite; the Ulyanjvsk igneous complex: 11 – dacite and diorite porphyry; 12 – normal fault; 13 – Cu > 0.3 aureole; 14 – contour of "loose-sulfide ores"; 15 – contour of the open pit for Summer, 2016.

277 pyrite grains from 8 samples from three areas in the northern part of the deposit have been studied to date. Site-1 is located in the central part of the main Cu-ore zone (Fig. 1), site-2 – in its western margin, and site-3 – outside of the ore boundary. The discovered inclusions and neogenesis represent the following mineral groups and types: 1) Native elements – gold and electrum, natural copper-zinc alloys (±Sn), iron; 2) Sulfdes – chalcopyrite, bornite, molybdenite, galena (usually Se-rich), sphalerite and (Fe,Cu,Zn)S phase, rarely arsenopyrite and argentite; 3) Sulfoarsenides of cobaltine- gersdorffite range (±Cu,Sb); 4) Sulfosalts – tennantite and tetrahedrite, very rarely in association with Bi- or Pb-Bi-sulfosalts; 5) Tellurides – hessite (predominant), Au-Ag-telluride which is close to petzite, coloradoite, altaite, tellurobismuthite; 6) Selenides and selenotellurides (Fig. 3 a) – naumannite (Ag_2Se), kurilite (Ag_8Te_3Se), unidentified phases or phase mixtures of Au-Ag-Se, Cu-Ag-Se, Ag-Pb-Se-(± Bi). Fine aggregates of selenides and tellurides are occasionally observed; sulfoselenides may be also present. Among the gangue minerals, most typical are newly formed monazite of variable composition, K/Na chlorides and more complex chloride compounds, inclusions and selveges of bitumen. The diagram (Fig. 2) shows comparative abundance of various inclusions in the three studied argillic alteration sites.

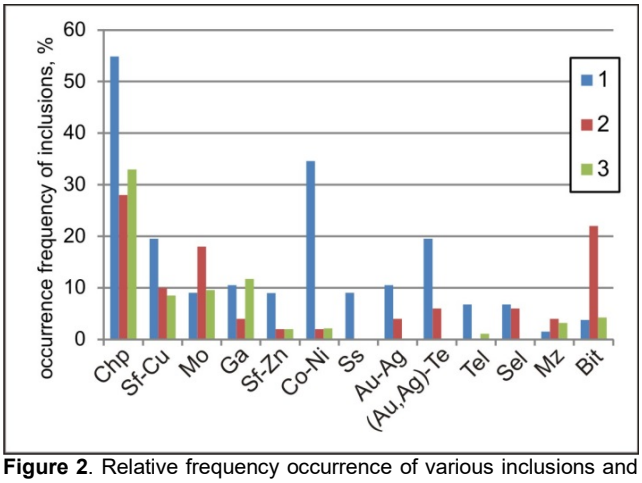

Figure 2. Relative frequency occurrence of various inclusions and neogenesises on the surface of pyrite grains from argillic metasomatites of Mikheevskoe deposit.
1, 2, and 3 – sampling areas in the northern part of the deposit. Key to mineral types and groups: Chp – chalcopyrite, Sf-Cu – copper sulphides (bornite ± chalcocite), Mo – molybdenite, Ga – galena, Sf-Zn – zinc sulphides (sphalerite, (Fe,Cu,Zn)S) phase, Co-Ni – sulpharsenides of cobaltite-gersdorffite range, Ss – sulfosalts, Au-Ag – native gold and electrum, (Au,Ag)-Te –gold and silver tellurides, Tel – other tellurides, Sel – selenides (mostly Au, Ag), Mz – monazite, Bit – bitumen

Pyrite from the central part of copper ore zone (site-1) is featured by the highest amount and variety of such inclusions; it is relatively enriched by Au-Ag minerals, and represents the only place where sulphosalts occur. Inclusions of molybdenite, monazite, and bitumen are more common in the periphery of the ore zone (site-2). The most "inclusion-poor" pyrite comes from argillic altered rock of site-3 which is outside of the main ore zone and, in particular, lacks any noble metal mineralization or selenides.

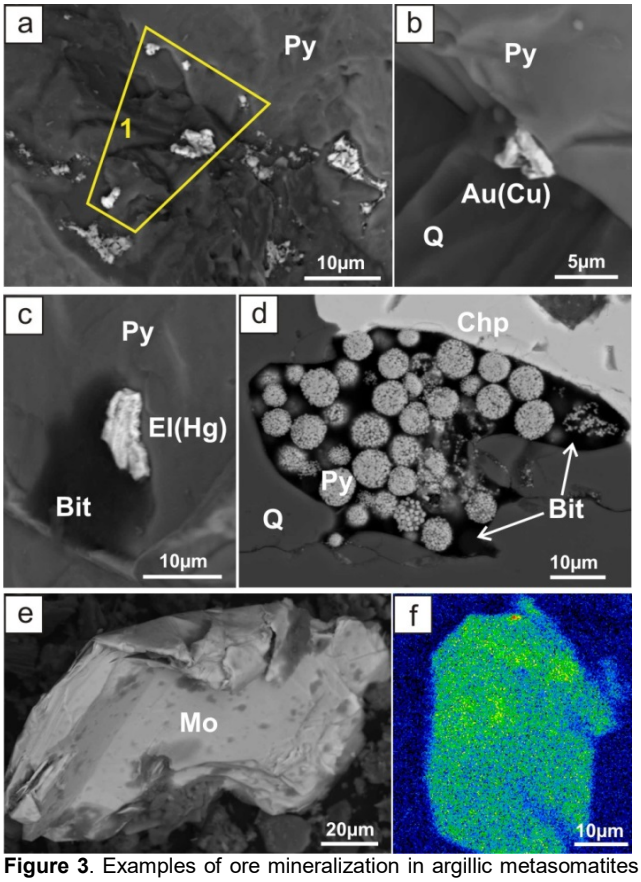

Figure 3. Examples of ore mineralization in argillic metasomatites of Mikheevskoe deposit.
a-c – inclusions on the pyrite surface (BSE images); **a** – selenide and telluride association: in Area-1 – phase close to fischesserite Ag_3AuSe_2 + native Au и hessite Ag_2Te, in the remaining part – mixture of naumannite Ag_2Se, hessite Ag_2Te, kurilite Ag_8Te_3Se and unidentified phases; **b** – inclusion of Cu-rich native gold without any silver (Cu 5.5 wt%); c – inclusion of Hg-rich electrum (Hg 10 wt%) in association with bitumen; **d** –pyrite framboids in a bitumen-filled cavity (polished thin section from siliceous area of argillic alteration, BSE image); **e** – molybdenite in loose argillic metasomatite (BSE image); **f** –(ReL_α X-ray map of molybdenite, Re content is from 0.22 to 0.93 wt%). Bit – bitumen, Chp – chalcopyrite, El – electrum, Mo – molybdenite, Py – pyrite, Q – quartz.

Native gold is present as micron-scale segregations ≤10 μm, both in polished thin sections of relatively intense argillic metasomatites, and on surface of pyrite from loose argillic metasomatites (Fig. 3 b,c). Unlike gold from the porphyry-style ore, this gold has a wide variation in fineness – from electrum and Hg-bearing electrum (fineness < 300, Hg up to 10 wt%) to quite high-fineness gold (Plotinskaya et al. 2018). Frequently there are intimate intergrowths of native gold and Au-Ag-tellurides and selenides. Cu-rich gold with 4-5 wt% of Cu and no Ag was noted in few specific cases; this, according to (Spiridonov and Pletnev 2002) suggests rather low-temperature conditions.

Molybdenite occurs in loose argillic metasomatites as platy parcel-like ~0.01-~0.1 mm (Fig. 3 e), sometimes larger, grains – often intergrown with pyrite. There are occasional molybdenite enriched zones associated with

argillic altered porphyry dikes. Rhenium distribution in molybdenite is rather uneven, patchy-spotted, with some zonation (Fig 3 f) and considerable variation of Re content (average 0.43 wt%), which, on the whole, corresponds to molybdenite from porphyry-style ore (Grabezhev 2013; Plotinskaya et al. 2015). The only difference is somewhat higher rhenium content in specific spots – up to 1.72 wt%.

Bitumen traces were identified in a significant number of samples. By burn-off temperature (exo-effect peaks on DTA curves) the bitumen corresponds to low-middle kerite – Tmax 305-375°C (Azovskova et al. 2015). Bitumen selvedges and inclusions observed on pyrite grains and other ore minerals are usually enriched by Cl, P, ± F, As. Sometimes they feature micro-inclusions of native gold, galena, native lead, and unidentified mineral phases (Fig. 3 c,d). Such mineralization is likely to be related to incomplete breakdown of organoelemental and chloride compounds and can indicate active involvement of organic matter in low-temperature process of argillic phase of mineralization-alteration.

4 Conclusions

Argillic metasomatites are present in variable volumes in most known porphyry copper deposits and can occur at different stages of porphyry system development (Sillitoe 2010). In the Mikheevskoe deposit such metasomatites are quite abundant, and even represent a special process type of ore in the upper section. They have distinctive ore- and accompanying mineralization (e.g. presence of Au-Ag, Ag, and Pb selenides, large variations of native gold composition, traces of low temperature bitumen etc.). Differences in mineral composition and the degree of accompanying mineralization between various areas of the deposit reflect element zonation which may be related both to argillic alteration and to earlier ore and alteration processes. Ore-bearing argillic rocks of Mikheevskoe deposit formed at the final epithermal stage of deposit formation however, certain influence of later endogenous processes during Late Mesozoic tectono-magmatic activation of Uralian structures cannot be excluded.

Acknowledgements

This study was supported by the state assignment projects of IGG UB RAS (theme 0393-2018-0031) and Russian Foundation for Basic Research, project # 19-05-00254. I.A. Gottman, L.V. Leonova, D.A., Zamyatin (IGG UB RAS, Yekaterinburg) are warmly thanked for their assistance with SEM and microprobe analysis. N.G. Petrishcheva, T.Ya. Gulyaeva and O.L. Galahova (IGG UB RAS, Yekaterinburg) are acknowledged for X-ray and TG/DTA analysis.

References

Azovskova OB, Malyugin AA, Nekrasova AA, Yanchenko MY (2013) Pyrite from zones of Mz-Kz reactivation of large faults on the eastern slope of the UralMountains, Russia. WASET Eng Technol (London) 79:463–467.

Azovskova OB, Rovnushkin MY, Glavatskikh SP (2015) Mineralogy of argillic altered rocks from the Mikheevskoe porphyry copper deposit, South Urals. Metallogeny of ancient and modern oceans−2015 21:116–120 (in Russian).

Grabezhev AI (2013) Rhenium in porphyry copper deposits of the Urals. Geol Ore Deposit 55:13–26.

Grabezhev AI (2014) Novonikolaevsk (Mo, Au)-Cu-porphyry ore area (Southern Ural, Russia): pertochemistry of ore-bearing granitoids and metasomatites. Lithosphere (Russia) 14(2):60–76 (in Russian with English abstract).

Grabezhev AI, Belgorodskii EA (1992) Ore-bearing granitoids and metasomatites of copper porphyry deposits. Nauka, Yekaterinburg (in Russian).

Plotinskaya OY, Azovskova OB, Abramov SS, Groznova EO, Novoselov KA, Seltmann R, Spratt J (2018) Precious metals assemblages at the Mikheevskoe porphyry copper deposit (South Urals, Russia) as proxies of epithermal overprinting. Ore Geol Rev 94:239–260.

Plotinskaya OY, Grabezhev AI, Seltmann R (2015) Rhenium in ores of the Mikheevskoe Mo-Cu porphyry deposit, South Urals. Geol Ore Deposit 57:118–132.

Puchkov VN (2010) Geology of the Urals and Cis-Urals (Actual Problems of Stratigraphy, Tectonics, Geodynamics and Metallogeny). DesignPoligraphService, Ufa (In Russian with English abstracts).

Russian Copper Company. http://rmk-group.ru/en/activities/enterprises/mikheevsky/ (accessed 10/03/2019).

Sillitoe RH (2010) Porphyry copper systems. Econ Geol 105:3–41.

Shargorodskii BM, Novikov IM, Aksenov SA (2005) The Mikheevskoe copper porphyry deposit in the South Urals. Otechestvennaya Geologia (2):57–61 (in Russian).

Spiridonov EM, Pletnev PA (2002) Zolotaya Gora auricupride deposit (about “gold-rodingite” formation). Nauchnyi Mir, Moscow (in Russian).

Tauson VL, Babkin DL, Pastushkova TN, Krasnoshchekova TS, Lustenberg EE, Belozerova OY (2011) Dualistic distribution coefficients in the system mineral-hydrothermal solution. I. Gold accumulation in pyrite. Geochem Int 49(6):568–577.

Tessalina SG, Plotinskaya OY (2017) Silurian to Carboniferous Re-Os molybdenite ages of the Kalinovskoe, Mikheevskoe and Talitsa Cu-Mo porphyry deposits in the Urals: implications for geodynamic setting. Ore Geol Rev 85:174–180.

Fluid evolution and genesis of epithermal gold deposit hosted by a shear-zone: Banská Hodruša, Slovakia

Peter Koděra, Alexander Kubač, Peter Uhlík, Rastislav Vojtko, Martin Chovan
Faculty of Natural Sciences, Comenius University

Jaroslav Lexa, Rastislav Milovský
Earth Science Institute, Slovak Academy of Sciences

Oscar Laurent
Department of Earth Sciences, ETH Zürich

Anthony E. Fallick
Scottish Universities Environmental Research Centre

Abstract. The Banská Hodruša gold deposit is hosted by a low-angle shear zone in the centre of a Neogene stratovolcano. The deposit developed during five mineralisation stages and two stages of shear zone evolution. Fluid inclusion and stable isotope data showed that temperature, chemical and isotopic composition of fluids were nearly constant during all mineralisation stages in all parts of the deposit. Precipitation of ores was triggered by boiling and cooling of fluids. The dominant source of fluids was contracted magmatic vapour mixed with deep-convecting meteoric water. The genetic model includes sequence of events starting with the emplacement of a granodiorite pluton, associated with Pb-Zn-Cu stockwork mineralization and advanced argillic alteration. It followed a rapid exhumation of the granodiorite and the shear zone evolution, which was penetrated by fluids, represented by contracted magmatic vapour mixed with deep-convecting meteoric water. Ore mineralisation is related to focusing of fluids in areas with a dense network of dilatational structures, while the argillised upper boundary of the shear zone worked as a collector of hydrothermal fluids and gases resulting from boiling. The final evolution includes caldera subsidence and long-lasting resurgent horst uplift, hosting an extensive system of younger veins.

1 Introduction

The intermediate-sulfidation Au-Ag-Pb-Zn-Cu deposit at the Rozália mine in Banská Hodruša represents an unusual subhorizontal multi-stage vein system, hosted by a low-angle normal fault zone (LANF). The shear zone, hosting the vein system, is related to processes of exhumation of a subvolcanic granodiorite pluton, probably accompanied by a sector collapse of the hosting stratovolcano (Kubač et al. 2018). The unusual structural setting of the deposit resulted in several unique characteristics, including fluid properties of the hydrothermal system, distribution of ores and alteration patterns. The proposed genetic model is based on new and published fluid inclusion and stable isotope data, interpreted in accordance with available geological, mineralogical and structural information.

2 Banská Hodruša deposit

The deposit is hosted by the central zone of the large Middle Miocene Štiavnica stratovolcano, the largest stratovolcano in the Central Slovakia Volcanic Field, located on the inner side of the Carpathian arc. The stratovolcano includes an extensive caldera, a late-stage resurgent horst in the caldera centre and an extensive pre- to syn-caldera subvolcanic intrusive complex. The gold mineralization is hosted by pre-caldera andesite, near to the flat roof of a pre-mineralisation subvolcanic granodiorite pluton. The veins are dismembered by a set of quartz-diorite porphyry sills and later steeply-dipping faults of the resurgent horst, mineralized with Cu-Pb-Zn epithermal ores.

The gold deposit occurs at the Rozália mine, 400–650 m below the surface. Epithermal gold ore has been exploited here since 1992, but in the past the Rozália mine was also used to exploit the horst-related Cu-Pb-Zn epithermal veins and base-metal stockwork mineralization. The stockwork mineralisation occurs some 1.5 km south of the Au-Ag deposit, hosted by apical porphyritic part of the granodiorite pluton and resembles a porphyry hydrothermal system including potassic alteration in the granodiorite, and advanced argillic alteration in the overlying andesite (Koděra et al. 2004).

The gold deposit consists of two parts, separated by a thick sill of post-mineralisation quartz-diorite porphyry. The western part has been already mined out but the eastern part is still exploited, with the annual production of ~30–45 kt of ore with 14 g/t Au, 17 g/t Ag, 0.6 wt% Zn, 0.45 wt% Pb, and 0.15 wt% Cu.

The deposit developed during five stages (Kubač et al. 2018). Stage 1 is related to hydraulic fracturing along subhorizontal structures dipping 20–30° to SE related to the underground cauldron subsidence and corresponds to the origin of low-grade silicified breccia at the base of the deposit. The major productive Stage 2 is related to the early evolution of the LANF with mostly southward movement of the downthrown block and is represented by a stockwork of steep veins (40–60° to S) with rhodonite-rhodochrosite (Stage 2a) and quartz-sulphide-carbonate (Stage 2b) assemblages with sphalerite, galena, chalcopyrite, pyrite, gold, rare hessite and

petzite. Locally, these veins are accompanied by quartz-gold veins resulting from complementary transtensive sinistral strike-slip movements (Stage 2c). Stage 3 is related to a renewed motion of the downthrown block towards the SE. The corresponding oriented vein systems consist of thin quartz-gold veins located on tension cracks inside the shear zone (dips ~45° to SE, Stage 3a), and complementary detachment-hosted quartz-base metals-gold veins (<30°; Stage 3b) located in the roof of the shear zone. Post-ore veins include rare barren quartz veins of variable orientation (Stage 4) and steep base metal veins with the NE-SW strike, related to the resurgent horst uplift (Stage 5).

Hydrothermal alteration occurs in a zonal arrangement (Koděra et al. 2017). Major veins are accompanied strong adularisation, quartz and illite. Strong argillisation occurs along the upper boundary of the shear zone there represented predominantly by illite, accompanied by quartz and pyrite. At the base of the deposit silicification of variable intensity is present, corresponding mostly to the Stage 1 mineralisation. Weak adularisation occurs in the hanging wall of silicites and close to minor ore veins. Propylitisation occurs distal to ore veins and in the hanging wall of the deposit (above the shear zone).

3 Methods

The new microthermometry on fluid inclusions was conducted on a Linkam THMSG-600 cooling-heating stage. LA-ICP-MS microanalyses of fluid inclusions were performed at the Department of Earth Sciences, ETH Zürich, with a Perkin Elmer NexION 2000 fast-scanning quadrupole ICP MS connected to a GeoLas 193 nm ArF excimer laser ablation system. The new $^{18}O/^{16}O$ and $^{13}C/^{12}C$ isotopic compositions were analysed at SUERC (Glasgow, UK), D/H at the Earth Sciences Institute of SAS in Banská Bystrica (Slovakia). For the stable isotope study of clays, the size fraction <2 μm or smaller was used, with mineralogy checked by XRD. The XRD analyses of clay fractions were also used for calculation of temperatures using expandability (smectite content in illite-smectites) and illite crystallinity (Kübler index – KI).

Data presentations and interpretations include fluid inclusion microthermometry and stable isotope data already published by Koděra et al. (2004, 2005) from the base metal stockwork mineralisation and epithermal mineralisation from the western part of the deposit.

4 Results

4.1 Fluid inclusions

Fluid inclusions from quartz, sphalerite and carbonates from the gold mineralisation are of low salinity (~1–3 wt.% NaCl eq.) and moderate homogenization temperatures (Th; ~250–310 °C) with frequent evidence of extensive boiling. No apparent differences occur between quartz data from both parts of the deposit, nor individual stages, except Stage 1 silicites which show slightly higher temperatures (up to 330 °C). Data from sphalerite show apparently lower mean Th values than quartz (~250–280 °C), but salinity is similar, so the changes in temperature can probably be explained by boiling (which is an endothermic process) rather than mixing. Sometimes carbonates from various stages also show lower Th values.

Fluid inclusions from the host-related veins (Stage 5) showed Th peaks at ~285 and 185 °C and salinities between 1 and 4 wt% NaCl eq., corresponding to two different substages in the vein filling. Evidence for boiling was observed locally (Koděra et al. 2005).

Hydrothermal minerals from the base metal stockwork mineralisation (epidote, sphalerite, calcite) host inclusions that showed progressive decrease in salinities (5 to 0.5 wt% NaCl eq.) and Th values (330 °C to 190 °C), indicative of fluid mixing. Data for massive silica from the overlying advanced argillic alteration (0.3–3.9 wt% NaCl eq., 240–360 °C) are consistent with the origin from magmatic condensates (Koděra et al. 2004).

The fluid inclusion populations with evidence for boiling were used to calculate fluid pressures and depths of formation. In the gold mineralization the highest fluid pressure was determined for Stage 1 inclusions (~85 bars), while the Stage 2 and Stage 3 inclusions showed very variable pressure estimates (45–80 bars). The highest pressure corresponds to initial opening of host fractures, when the hydrothermal system was governed by suprahydrostatic conditions, probably with a lack of connection to the surface. Local overpressure is indicated by frequent breccia textures in silicites. Variable pressures are indicative of local decompression in dilatational structures, with pressure release resulting in extensive boiling, followed by precipitation of gold, adularia and Mn-minerals. The calculated apparent paleodepths, corresponding to changes in fluid pressure, are also very variable due to the local suprahydrostatic conditions and possible variation in CO_2 content. The probable paleodepth (550 ± 100 m) can be derived from the lowest fluid pressure value. Inclusions from Stage 5 steep horst-related veins produced pressures 60–68 bars, corresponding to 780 ± 60 m at hydrostatic conditions.

Results of LA ICPMS analyses of fluid inclusions from the gold deposit showed that (i) the same set of elements is systematically detected (Na, B, Cl, K, As, Rb, Sr, Sb, Cs ± Fe, Cu, Zn, Au, Pb); and (ii) the ratios of these elements to Na are fairly homogeneous, despite the low salinity and small size of most inclusions. Both are clear evidences that the fluids had a common, long-lasting source throughout the entire hydrothermal process and precipitation of ore mineralisation was mostly affected by pressure decrease and cooling rather mixing of fluids. High B/Rb, B/Sr and As/Rb ratios indicate that contracted magmatic vapour was the dominant source of hydrothermal fluids, with no or little influence of fluid/rock reaction with sedimentary rocks (c.f. Large et al. 2016). Fluids in pre-mineralisation stages (1 and 2a) had probably a higher proportion of the contracted magmatic vapour compared to later stages, as indicated by their relatively higher B, As, Sb contents, Na/K values and lower Cl, Rb and K contents than later stages. This can be explained by the fact that both B, As and Sb are known to preferentially accumulate in vapour, while Rb and K are

affiliated to magmatic brines (Pokrovski et al. 2002). The relatively higher proportion of contracted vapour in early stages also corresponds to their slightly lower salinity but higher Th values. Gold content in fluids typically ranges from 0.2 to 2 ppm; however, some individual inclusions have sometimes significantly higher concentrations up to 50 ppm. The increased gold contents were determined in fluid inclusions from all gold bearing stages (2b, 3a, 3b), as well as in Stage 5 horst-related veins. Silver/gold ratio in fluid inclusions was similar to most gold ores at the deposit, i.e. close to 10.

4.2 Stable isotopes

Oxygen isotope data from vein quartz and illites associated with gold mineralisation suggest a relatively narrow range of $\delta^{18}O_{fluid}$ values (-2 to 1 ‰) for all stages of veins and for both the western and eastern parts of the deposit. Fluids in equilibrium with illite are also very homogeneous in terms of hydrogen isotope ratio (-50 to -69‰ δD_{fluid}). This indicates that the source fluid was quite homogeneous, which is consistent with the low variability of fluid inclusion data, including Th values and chemical composition, during all mineralisation stages in all studied parts of the deposit. Only the fluids associated with Stage 1 silicites and illites are isotopically slightly heavier (by ~1 ‰) compared to other stages. A somewhat different composition is only indicated by carbonates that show slightly lower $\delta^{18}O_{fluid}$ values (-1.9 to -2.7 ‰).

Isotopic composition of epithermal fluids plotted in a $\delta^{18}O_{fluid}$ vs. δD_{fluid} diagram shows a mixed character of fluids falling between the fields of typical magmatic water dissolved in felsic melts and meteoric waters. The observed well homogenised fluid composition is consistent with mixing of the fluids outside of the deposit during ascent of magmatic fluids from depth, assuming a deep-convecting source of meteoric fluids.

The isotopic signature of the hydrothermal alteration of granodiorite that is associated with the base metal stockwork mineralization was examined using epidote and chlorite (0.4 to 1.1 ‰ $\delta^{18}O_{fluid}$, -22 to -46 ‰ δD_{fluid}; Koděra et al. 2004). Fluids related to accompanying advanced argillic alteration were characterised by analyses of illite, illite-smectite and massive silica (-8.2 to 0.6 ‰ $\delta^{18}O_{fluid}$, -64 to -50 ‰ δD_{fluid}). In contrast to epithermal veins, the data show a progressive mixing trend of magmatic fluids with $\delta^{18}O$-shifted meteoric waters. The isotopic composition of meteoric water in this system was roughly similar to that in the epithermal vein system and it is also similar to the present-day meteoric water. The mixing trend is probably related to a relatively shallow convection of meteoric water in the vicinity of a thermal anomaly of ascending, predominantly magmatic hydrothermal fluids in the apical part of the pluton. They include early magmatic vapour that has condensed in overlying andesite and resulted in advanced argillic alteration, and later supercritical magmatic fluid, responsible for the base metal stockwork mineralisation (Koděra et al. 2004). However, contracted magmatic vapour could be an alternative form of magmatic fluid source.

4.3 Illite geothermometry

The XRD analyses of clay fraction were used for calculation for crystallisation temperatures of clay minerals (illite, illite-smectite). Illite from the vicinity of veins provided KI values from ~0.4 to 0.6, corresponding to temperatures from 270 to 290 °C, which are similar to fluid inclusion homogenization temperatures. Especially, the illite from the hanging-wall of the detachment-hosted vein system (Stage 3b) has a nearly constant crystallinity for all studied samples, similar to their oxygen isotope data. This indicates that there was no apparent thermal gradient along this horizon.

Clays from the stockwork-related advanced argillic alteration produced significantly higher KI values of illites (0.7 to 1.3) and high proportion of smectite in illite-smectite (25 %), resulting in much lower temperature range of their crystallisation (135–248 °C). This corresponds to the mixing trend determined for this system using the stable isotope data.

5 Genesis of the deposit

The available geological, structural, mineralogical and fluid properties data obtained in this study enable to present a genetic model of the epithermal gold deposit at the Rozália mine (Fig. 1). The sequence of events started with the emplacement of the granodiorite bell jar pluton at a minimum depth of ~2 km (Konečný et al. 2002). The emplacement was accompanied by advanced argillic alteration in the overlying andesite, resulting from condensation of magmatic vapour escaping from the crystallising granodiorite magma. Mixing with meteoric water in the vicinity of the upflow zone has also occurred. Following cooling and fracturing of the apical part of the pluton, Pb-Zn-Cu stockwork mineralization precipitated here due to the upflow of a deep-exsolved supercritical fluid or magmatic vapour contracted to aqueous liquid. Neither the advanced argillic nor the stockwork system contain gold and precipitation of base metals occurred by mixing with external meteoric water.

Shortly after its emplacement, the granodiorite pluton has experienced a very rapid exhumation, followed by unroofing and low-angle normal shear zone evolution, possibly enabled by argillised nature of the overlying andesite. The shear zone was penetrated by hydrothermal fluids forming the Au-Ag ± Pb-Zn-Cu veins, followed by emplacement of quartz-diorite porphyry dikes and sills into the same structures. As indicated by the fluid inclusion data, the source of fluids was predominantly vapour escaping from the parental differentiated magma chamber. Vapour has contracted to liquid and mixed with deep-convecting meteoric water

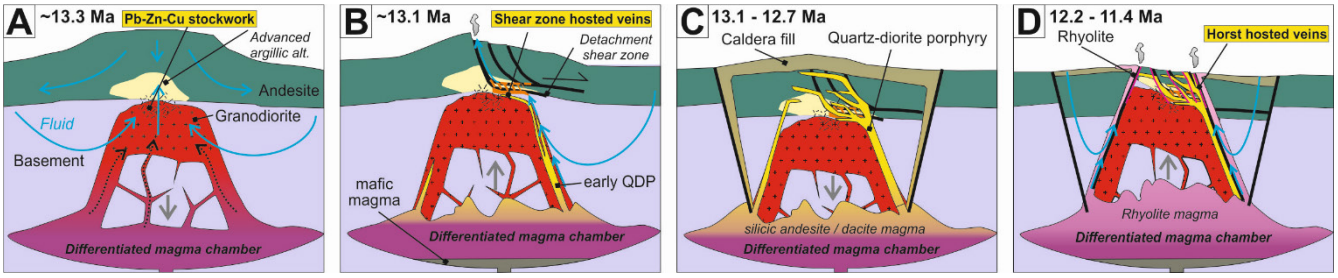

Figure 1. Stages and timing of geological evolution related to various mineralisation types at the Rozália mine, including corresponding fluid-flows. Ages are based on Chernyshev et al. (2013). A. Intrusion of granodiorite pluton with emplacement of base metal stockwork mineralization and associated advanced argillic alteration. B. Quick unroofing of the granodiorite and evolution of low-angle, normal shear zone hosting gold-bearing veins (Stages 1 to 4). C. Emplacement of quartz-diorite porphyry dikes and sills, followed by caldera subsidence later filled by andesite. D. Resurgent horst uplift in the caldera centre hosting the system of horst-related epithermal veins (Stage 5).

before reaching the shear zone level. Some admixed proportion of brine could have been also present in the fluid. Enrichment of fluids in gold probably resulted from the ability of vapour to transport gold, and possibly due to the degassing of a mafic magma that could have penetrated the parental magma chamber, as indicated by the presence of mafic nodules in post-mineral quartz-diorite porphyry sills. Precipitation of ores was triggered by boiling of fluids evolving from suprahydrostatic to hydrostatic conditions at a depth of ~550 m. Precipitation of ores usually started with precipitation of sulphides due to cooling, as boiling is an endothermic process. Subsequent precipitation of gold resulted from the resulting lack of sulphur in the fluid as gold in epithermal systems is mostly transported in sulphur complexes.

The main migration of paleofluids occurred along low-angle normal faults of the shear zone from S-SE to N-NW, as indicated by the geological setting of the quartz-diorite porphyries that intruded the shear zone at the end of the hydrothermal activity from S-SE. Main ore mineralisation is related to focusing of fluids in areas with a dense network of dilatational structures, where both major boundaries of the shear zone were relatively close together, i.e. where the hanging-wall argillite was relatively close to foot-wall silicite (Koděra et al. 2017). Opening of dilatational structures enabled an active suction of fluids and their boiling due to the decreased pressure. The strongly argillised upper boundary of the shear zone probably worked as a collector of hydrothermal fluids flowing along the shear zone and producing the Stage 3b veins, as well as a collector of vapour and gases escaping from boiling fluids throughout the entire thickness of the shear zone. Thus, this horizon is quite important for future exploration as it marks areas with extensive boiling (and possibly associated gold mineralisation) in the footwall of this argillised horizon.

The fluid-mixing trends obtained from isotopic data point to a similar meteoric water isotopic composition both for the granodiorite-related hydrothermal system and for the epithermal gold system. This interpretation is consistent with the assumed very quick exhumation of the granodiorite followed by shear zone development, as there was no time for significant change in the isotopic composition of meteoric water through changes in climate. Recent U-Pb dating has confirms that the exhumation has occurred in less than 0.3 Ma (unpublished work).

The final evolution of the deposit includes caldera subsidence, followed by the long-lasting resurgent horst uplift producing the extensive system of horst-related veins (Stage 5). The gold deposit was overlain by new portions of differentiated andesite (caldera-fill and post-caldera), which explains deeper boiling depth of the horst related veins (~780 m), compared to gold veins (~550 m).

Acknowledgements

This work was supported by the grants VEGA No. 1/0560/15, APVV-15-0083 and the company Slovenská banská, spol. Ltd.

References

Chernyshev IV, Konečný V, Lexa J, Kovalenker VA, Jeleň S, Lebedev VA, Goltsman YuV (2013) K-Ar and Rb-Sr geochronology and evolution of the Štiavnica Stratovolcano, Central Slovakia. Geol Carpath 64:327-351.

Koděra P, Lexa J, Rankin AH, Fallick AE (2004) Fluid evolution in a subvolcanic granodiorite pluton related to Fe and Pb-Zn mineralization, Banská Štiavnica ore district, Slovakia. Econ Geol 99:1745-1770.

Koděra P, Lexa J, Rankin AH, Fallick AE (2005) Epithermal gold veins in a caldera setting: Banská Hodruša, Slovakia. Miner Depos 39:921-943.

Koděra P, Kubač A, Uhlík P, Osacký M, Vojtko R, Chovan M, Lexa J, Žitňan P (2017) Hydrothermal alteration of a shallow-dipping epithermal Au-Ag-Pb-Zn-Cu deposit Banská Hodruša, Slovakia. Proc 14th SGA Bien Meeting, Québec City, Canada, Vol 1: 159-162.

Konečný P (2002) Evolution of magmatic reservoir underneath the Štiavnica stratovolcano (in Slovak). Unpubl PhD Thesis, Comenius Univ, Bratislava.

Kubač A, Chovan M, Koděra P, Kyle JR, Žitňan P, Lexa J, Vojtko R (2018) Mineralogy of the epithermal precious and base metal deposit Banská Hodruša at the Rozália mine (Slovakia). Miner Petrol 112:705–731.

Large SJE, Bakker EYN, Weis P, Wälle M, Ressel M, Heinrich CA (2016) Trace elements in fluid inclusions of sediment-hosted gold deposits indicate a magmatic-hydrothermal origin of the Carlin ore trend. Geology 44:1015-1018.

Pokrovski GS, Zakirov IV, Roux J, Testemale D, Hazemann J, Bychkov AY, Golikova GV (2002) Experimental study of arsenic speciation in vapor phase to 500 °C: Implications for As transport and fractionation in low-density crustal fluids and volcanic gases. Geochim Cosmochim Acta 66:3453–3480.